Full title: Loss of pseudouridine synthases in the RluA family causes hypersensitive nociception in *Drosophila*

Wan Song[1,2] & W. Daniel Tracey[1,2,*]

[1]Gill Center for Biomolecular Research, Indiana University, Bloomington, Indiana, USA

[2]Department of Biology, Indiana University, Bloomington, Indiana, USA

11 **Short title: Pseudouridine synthases in nociception**

12

13 **Key words:** *Drosophila melanogaster*, pseudouridine, nociception, behavior,

14 hyperalgesia, pain, dendrite, sensory neuron

15

16 * Corresponding author:

17 W. Daniel Tracey

18 The Linda and Jack Gill Center for Biomolecular Science

19 Indiana University

20 Multidisciplinary Science Building II (MSBII)

21 702 North Walnut Grove Avenue, Rm.106

22 Bloomington, IN 47405

23 Phone: (812) 856-2574

24 Email: dtracey@indiana.edu

Abstract

Nociceptive neurons of *Drosophila melanogaster* larvae are characterized by highly branched dendritic processes whose proper morphogenesis relies on a large number of RNA-binding proteins. Post-transcriptional regulation of RNA in these dendrites has been found to play an important role in their function. Here, we investigate the neuronal functions of two putative RNA modification genes, *RluA-1* and *RluA-2*, which are predicted to encode pseudouridine synthases. *RluA-1* is specifically expressed in larval sensory neurons while *RluA-2* expression is ubiquitous. Nociceptor-specific RNAi knockdown of *RluA-1* caused hypersensitive nociception phenotypes, which were recapitulated with genetic null alleles. These were rescued with genomic duplication and nociceptor-specific expression of *UAS-RluA-1-cDNA*. As with *RluA-1, RluA-2* loss of function mutants also displayed hyperalgesia. Interestingly, nociceptor neuron dendrites showed a hyperbranched morphology in the *RluA-1* mutants. The latter may be a cause or a consequence of heightened sensitivity in mutant nociception behaviors.

Author Summary

Pseudouridine (Psi) is a C5-glycoside isomer of uridine and it is the most common posttranscriptional modification of RNAs, including noncoding tRNAs, rRNAs, snRNAs as well as mRNAs. Although first discovered in the 1950s, the biological functions of Psi in multicellular organisms are not well understood. Interestingly, a marker for sensory neurons in *Drosophila* encodes for a putative pseudouridine synthase called RluA-1. Here, we report our characterization of nociception phenotypes for larvae with RluA-1 loss of

46 function along with that of a related gene RluA-2. Disrupting either or both RluA-1 and
47 RluA-2 resulted in hypersensitive nociception. In addition, RluA-1 mutants have more
48 highly branched nociceptor neurites that innervate the epidermis. Our studies suggest
49 an important role for the RluA family in nociception. This may be through its action on
50 RNAs that regulate neuronal excitability and/or dendrite morphogenesis.
51

52 ## Introduction

53 Pain serves an indispensable, protective role but when pain becomes
54 pathological it can have a debilitating impact on human life. The total annual cost of pain
55 to society in the United States was estimated by the Institute of Medicine to be up to
56 $635 billion, which is greater than that of heart disease, cancer, and diabetes combined
57 (Gaskin and Richard 2012). It is therefore of urgent importance to uncover the basic
58 molecular and cellular mechanisms involved in pain in order to better treat it. Laboratory
59 animal models of pain and nociception have played an essential role in identifying such
60 mechanisms. *Drosophila* larvae respond to noxious thermal and mechanical stimuli
61 through stereotyped rolling escape locomotion (in which the larva rotates around its long
62 body axis), which is robust and easily distinguishable from other forms of locomotion
63 (Tracey, Wilson et al. 2003). Rolling is used as a behavioral defense against attacks by
64 parasitoid wasps which lay their eggs within the fly larvae using a sharp ovipositor
65 (Hwang, Zhong et al. 2007). Successful wasp infection is lethal to the larvae and is a
66 strong selective pressure in natural populations of *Drosophila.* Combined with the

67 unparalleled genetic tools available for *Drosophila melanogaster*, this behavioral readout
68 provides an excellent system to study the genetics of nociception and pain (Tracey,
69 Wilson et al. 2003, Caldwell and Tracey 2010, Im and Galko 2012, Milinkeviciute, Gentile
70 et al. 2012, Tracey 2017, Khuong, Wang et al. 2019). Previous studies have demonstrated
71 a specific subset of dendritic arborization (da) sensory neurons in the peripheral nervous
72 system, Class IV multidendritic da (cIVda) neurons, are of critical importance for thermal,
73 mechanical and high intensity light nociception (Grueber, Jan et al. 2002, Hwang, Zhong
74 et al. 2007, Xiang, Yuan et al. 2010). Further evidence suggests a lesser but significant
75 contribution of Class II (cIIda) and Class III da (cIIIda) neurons in mechanical nociception
76 (Hwang, Zhong et al. 2007, Kim, Coste et al. 2012, Hu, Petersen et al. 2017). In addition,
77 great progress has been made in identifying the circuits in the larval abdominal ganglion
78 that are involved in rolling escape locomotion (Ohyama, Jovanic et al. 2013, Ohyama,
79 Schneider-Mizell et al. 2015, Chin and Tracey 2017, Burgos, Honjo et al. 2018).

80 Genes that are specifically expressed in multidendritic (md) neurons have been
81 found to play a role in nociception. For instance, *painless* (Tracey, Wilson et al. 2003) is
82 required for mechanical and thermal nociception and it is expressed in all four classes of
83 md neurons. Similarly, *straightjacket* (Neely, Hess et al. 2010) is expressed in md neurons
84 and required for avoidance of noxious heat. Mechanical nociception genes such as
85 *pickpocket* (Zhong, Hwang et al. 2010), *ppk26/balboa* (Gorczyca, Younger et al. 2014,
86 Mauthner, Hwang et al. 2014) and the polymodal nociception gene *dTRPA1-C/D* (Zhong,
87 Bellemer et al. 2012) each show very specific expression in the cIVda neurons. Forward
88 genetic screens have also identified a set of genes with enriched expression in the cIVda

89 neurons which either inhibit or activate nociceptive pathways (Honjo, Mauthner et al.
90 2016).

91 The historically first known genetic marker with specific expression pattern in the
92 da neurons was the *lacZ* enhancer trap *E7-2-36* (Brewster and Bodmer 1995). Later
93 studies reported that this enhancer trap gene was inserted upstream of the *RluA-1* gene
94 and DNA sequences from upstream of *RluA-1* caused expression of GAL4 in
95 multidendritic neurons (Wang, Lo et al. 2011). The *RluA1* gene encodes an enzyme that
96 is predicted to have pseudouridine synthase activity, but how this RNA modifying protein
97 is involved in the function of nociceptive multidendritic neurons remains unknown.

98 A widespread importance of RNA-binding proteins in cIVda neuron dendrite
99 morphogenesis and function was found in a recent large-scale RNAi screen that
100 identified 88 genes encoding RNA-binding proteins whose knockdown caused aberrant
101 dendrite morphogenesis (Olesnicky, Killian et al. 2014). The elaborate dendrite arbors of
102 cIVda neurons project long distances from the neuronal cell body and mRNA granules
103 are trafficked to these distant sites where they may undergo local translation. Indeed,
104 RNA granules containing Nanos (Nos), Pumilio (Pum), Oskar (Osk), Fragile X Mental
105 Retardation (FMRP) and other proteins have been shown to regulate the formation of
106 higher order dendrites in these cells (Pan, Zhang et al. 2004, Ye, Petritsch et al. 2004,
107 Brechbiel and Gavis 2008, Bianco, Dienstbier et al. 2010, Xu, Brechbiel et al. 2013).
108 Interestingly, the *nos* mRNA itself is transported into dendrites via a pathway that relies
109 on Oskar and Rumplestiltskin, two proteins that also play a role regulating *nos* in the

110 early embryo (Xu, Brechbiel et al. 2013). Mechanical nociception defects are also
111 observed in animals with disruption in these pathways (Xu, Brechbiel et al. 2013).

112 Pseudouridylation is the most common post-transcriptional RNA modification.
113 Pseudouridine (Ψ), the C5-glycoside isomer of uridine, was initially found in many
114 positions in rRNA, tRNA and snRNA in all organisms that have been investigated (Ge
115 and Yu 2013). RNA-seq based global pseudouridine profiling has shown the presence of
116 Ψ in many mRNAs and a large number of those sites were found to be dynamically
117 regulated in yeast and human cells (Carlile, Rojas-Duran et al. 2014, Lovejoy, Riordan et
118 al. 2014, Schwartz, Bernstein et al. 2014, Khoddami, Yerra et al. 2019). Dysfunctional
119 pseudouridylation has been linked to several human diseases (Knight, Heiss et al. 1999,
120 Fujiwara and Harigae 2013, de Brouwer, Abou Jamra et al. 2018). Since many sites of
121 pseudouridylation in different organisms are evolutionarily conserved, *Drosophila*
122 *melanogaster* may provide an excellent and genetically tractable metazoan system to
123 elucidate some of these functions.

124 The isomerization of uridine to pseudouridine is catalyzed by six families of
125 pseudouridine synthases. They function either as guide RNA directed ribonucleoprotein
126 complexes or as stand-alone proteins (Koonin 1996, Hammal and Ferre-D'Amare 2006).
127 In the *Drosophila* genome, 9 proteins have been identified with annotated
128 pseudouridine synthase domains. Minifly (mfl), the RNA-dependent pseudouridine
129 synthase homolog of human dyskerin (mouse NAP57 and yeast Cbf5), is required for
130 somatic stem cell homeostasis and is essential for *Drosophila* viability and fertility (Phillips,
131 Billin et al. 1998, Giordano, Peluso et al. 1999, Vicidomini, Petrizzo et al. 2017). Knockout

132 of *Drosophila* Pus7, the human and yeast Pus7 homolog, results in increased
133 aggressiveness in adult flies (de Brouwer, Abou Jamra et al. 2018). The function and
134 specificity of other predicted pseudouridine synthases are largely unknown. Among the
135 six families, the RluA family, which does not rely on guide RNAs, appears to be the most
136 complex based on divergent substrate specificities in bacteria and yeast (Hoang, Chen
137 et al. 2006). RluA family members in bacteria are involved in ribosomal assembly and
138 growth (Raychaudhuri, Niu et al. 1999, Gutgsell, Deutscher et al. 2005) but their function
139 in multicellular organisms has not been studied. Although pseudouridine synthases
140 appear to function ubiquitously, as noted above, *Drosophila RluA-1*, a member in RluA
141 family, has been reported to be specifically expressed in md neurons (Wang, Lo et al.
142 2011). Thus, we have investigated the role for *RluA-1* and its paralog *RluA-2*, in
143 nociception pathways that are known to depend on md neurons. Our results indicate an
144 important function for *RluA-1* and *RluA-2* in the regulation of nociception.

145 ## Results

146 ### *RluA-1* is expressed in the multidendritic neurons of the peripheral nervous
147 system and in the cells of brain

148 Previously described reporter genes for *RluA-1* showed specific expression in
149 larval multidendritic neurons (Wang, Lo et al. 2011). We replicated this finding by
150 generating an *RluA-1*^{GAL4} driver at the endogenous gene locus through recombination
151 mediated cassette exchange (RMCE) of *RluA-1*^{MI06897} (an intronic MiMIC) and a Trojan
152 exon cassette (Diao, Ironfield et al. 2015). An mCD8GFP reporter driven by *RluA-1*^{GAL4}

153 was expressed in peripheral sensory neurons in each segment of the larval body wall
154 (**Figure 1A**). In the dorsal cluster, GFP-positive signals were clearly detected in all four
155 classes of md-da sensory neurons, dorsal multiple dendrite neuron (dmd1), external
156 sensory (ES) and dorsal bipolar dendritic (dbd) neurons (**Figure 1B**). In the larval ventral
157 nerve cord, the GFP-positive signals were seen in the axonal projections of the sensory
158 neurons (**Figure 1C**). GFP signal was also observed in the unidentified clusters of neurons
159 in the larval brain (**Figure 1C).** In the adult brain, significant signals were detected in the
160 optic lobes and other small cell clusters of the central brain (**Figure S1A)**.

161 To determine the localization of the RluA-1 proteins, we generated a GFSTF exon
162 trap (Nagarkar-Jaiswal, DeLuca et al. 2015) that expresses an in frame GFP fusion with
163 *RluA-1* at the endogenous genomic locus (with RMCE of the *RluA-1*^{MI06897} MiMIC element)
164 (Nagarkar-Jaiswal, DeLuca et al. 2015). Although live imaging did not detect the EGFP
165 tagged RluA-1 protein, immunostaining with anti-GFP labelled nuclei of larval
166 multidendritic neurons, ES and dbd neurons also expressing a membrane-localized RFP
167 (*Gal4109(2)80 > UAS-CD8-RFP*, **Figure 1D**). The tagged RluA-1 protein was also
168 detected in the cell bodies of neurons in optic lobes and other yet-to-be identified cells
169 in the adult brain (**Figure S1B**).

170 **Reducing or removing *RluA-1* results in a hypersensitive thermal nociception**
171 **phenotype**

172 Given our confirmation of the expression of the *RluA1* gene and protein in the
173 multidendritic neurons we tested for potential roles of RluA-1 in the regulation of

174 nociception. To do so, we first performed tissue-specific knockdown using GAL4/UAS
175 based RNA interference (RNAi). A cIVda specific driver (*ppk1.9-GAL4 UAS-dicer2*)
176 (Ainsley, Pettus et al. 2003) was employed to drive an *RluA-1* RNAi construct in the larval
177 cIVda nociceptors. We assessed potential insensitive phenotypes (with a probe
178 temperature of 46°C) and potential hypersensitive phenotypes (with a temperature of
179 42°C) as previously described (Honjo, Mauthner et al. 2016). When stimulated with the
180 higher temperature 46°C probe the *RluA-1-RNAi* larvae responded significantly faster
181 than the *ppk-GAL4* driver alone controls. This genotype also responded faster than the
182 UAS-RNAi controls but this difference was not statistically significant (**Figure 2A**). The
183 results suggested that reducing *RluA-1* in classIV neurons may have made the larvae
184 more sensitive to noxious heat. Indeed, a clearly hypersensitive phenotype for the *RluA1-*
185 RNAi animals was seen when testing with 42°C probe (**Figure 2A**). The average latency
186 to roll in the *RluA-1* knock-down animals was significantly faster than the driver alone
187 animals or the *UAS-RNAi* control animals. These data combined suggest that reducing
188 the activity of *RluA-1* in the noxious heat-responsive cIVda cells caused thermal
189 hyperalgesia.

190 To further test the function of *RluA-1* we next generated a precise genetic
191 deletion mutant of *RluA-1* in which 11.14 kbp including the entire *RluA-1* genomic region
192 was removed by CRISPR-guided homologous recombination-directed repair (HDR) (Ran,
193 Hsu et al. 2013). Homology arms of ~1kb immediately flanking the CRIPSPR cleavage
194 sites were used to direct the HDR (**Figure S2A**). The resultant deletion mutant (*RluA-1*$^{del-}$
195 ^{HDR}) was confirmed by PCR amplification and sequencing of PCR products from the

196 targeted *RluA-1* locus (**Figure S2B and S2C**). To facilitate the behavioral comparisons,
197 the *RluA-1*$^{del\text{-}HDR}$ mutant was backcrossed six times to our most commonly used genetic
198 background strains Canton-S (CS), *w*^{1118}, and isogenized *w*^{1118} (iso*w*^{1118}). As with class IV
199 md neuron-specific RNAi knockdown, *RluA-1*$^{del\text{-}HDR}$ larvae showed significantly faster
200 responses to noxious heat stimulation of 42°C compared to the corresponding control
201 animals, regardless of genetic background (**Figure 2B**). Note that for unknown reasons,
202 these genetic backgrounds vary in their baseline responses. This genetic background
203 effect has a significant impact on the latency of larval nociception responses to noxious
204 heat stimuli, with the most striking differences between homozygous *RluA-1*$^{-/-}$ and the
205 relatively insensitive iso*w*^{1118} background, followed by that of *w*^{1118} background, and then
206 the CS background (**Figure 2B**).

207 Given the sensitivity to genetic background, we performed an additional genetic
208 test for the importance of *RluA-1*, by generating an independent mutant allele
209 (*RluA-1*$^{del\text{-}FRT}$) using FLP recombinase and FRT-bearing insertions (Parks, Cook et al. 2004)
210 (*PBac{WH}*^{f02750}(+) and *p{XP}*^{d2586}(-), **Figure S2A**). Transheterozygous *RluA-1*$^{del\text{-}FRT}$/*RluA-1*$^{del\text{-}HDR}$
211 mutant larvae displayed hypersensitivity to a 42°C stimulus (**Figure 2C**)) indicating
212 that *RluA-1*$^{del\text{-}FRT}$ failed to complement *RluA-1*$^{del\text{-}HDR}$. Failure of complementation of
213 independently generated alleles created in distinct genetic backgrounds provides strong
214 evidence that the hypersensitive nociceptive phenotypes observed are a consequence
215 of the mutation of *RluA-1* and not due to unlinked mutations present in one background
216 or another.

217 For the remainder of our behavioral studies, we relied on the isogenized w^{1118}
218 background. This had the advantage of greater genetic uniformity relative to w^{1118} and
219 CS, as well as showing the strongest hypersensitive mutant phenotype for *RluA-1*.

220 **Genetic rescue of *RluA-1* mutant restores thermal nociception response**

221 To test that the mutation in *RluA-1* was the underlying cause of the hypersensitive
222 nociception phenotype, we introduced a genomic rescue construct into the *RluA-1*$^{del\text{-}HDR}$
223 mutant background (a Bacterial Artificial Chromosome (BAC) (P6-D7)) (Venken, Carlson
224 et al. 2009) covering the *RluA-1* gene region). With the 42°C stimulus, larvae with two
225 copies of the duplication (Dp) in the background of *RluA-1*$^{del\text{-}HDR}$ showed rescue of the
226 hypersensitivity (**Figure 3A**). This rescue with the genomic duplication was dosage
227 dependent. Larvae with only one copy of the Dp in the *RluA-1*$^{del\text{-}HDR}$ background (*RluA-1*$^{-}$
228 $^{/-}$; *Dp*$^{+/-}$) responded more slowly than the mutant this difference was not statistically
229 significant (**Figure 3A**). Combined, the results of genomic rescue experiments support
230 the hypothesis that mutation of *RluA-1* is indeed the cause of the hypersensitive thermal
231 nociception phenotype.

232 A caveat remained in that the genomic rescue construct included other genes in
233 addition to *RluA-1*. Thus, genomic rescue did not rule out the possibility that a mutation
234 tightly linked to *RluA-1,* but not in *RluA-1* itself, was responsible for the mutant
235 phenotype. Thus, as a final test, we generated transgenic lines to express an *RluA-1*
236 cDNA under the control of the GAL4/UAS system (*UAS-RluA-1*). Using the *UAS-RluA-1*
237 we specifically restored *RluA-1* to cIVda neurons in the *RluA-1* null mutant background.

238 When stimulated with the 42°C probe the animals with both the *ppkGal4* driver and the
239 *UAS-RluA-1-cDNA* transgene in the *RluA-1* $^{del\text{-}HDR}$ showed a complete rescue from the
240 hypersensitivity seen in the null mutant (**Figure 3B**). Neither the *ppkGal4* driver alone
241 nor the *UAS-RluA-1* had an effect on the hypersensitive thermal nociception phenotype
242 in the *RluA-1* null mutant background, excluding the possibility of non-specific effects of
243 these transgenes (**Figure 3B**). In addition, overexpression of *UAS-RluA1* with a md
244 neuron driver (MD-Gal4) had no effect on nociception behavior at 42°C stimulus ruling
245 out the possibility that the increased latency seen in the rescue effect was a non-specific
246 consequence of over-expression (**Figure S3**). Combined, these nociceptor-specific
247 rescue experiments provide genetic confirmation that loss-of-function mutation in *RluA-*
248 *1* causes hypersensitive thermal nociception and localizes the site of action for RluA-1 in
249 this process to the nociceptors.

250 ***RluA-1* requirement for mechanosensory thresholds**

251 The cIVda neurons are not only required for detection of noxious heat, they also
252 contribute to sensing harsh mechanical stimulation (Hwang, Zhong et al. 2007, Zhong,
253 Hwang et al. 2010, Mauthner, Hwang et al. 2014). Thus, we investigated the *RluA-1*
254 mutant responses to noxious mechanical stimuli. When stimulated with a 30mN/720kPa
255 Von Frey fiber, significantly more *RluA-1* $^{del\text{-}HDR}$ null mutant larvae performed the typical
256 nociceptive rolling behavior compared to the isow^{1118} controls (**Figure 4A**). Even when
257 the probe strength/pressure was reduced to 15mN/360kPa, the majority of *RluA-1*$^{-/-}$
258 larvae still rolled while less than half of control larvae rolled (**Figure 4A**), indicating the

259 defect in *RluA-1* also caused hypersensitive mechanical nociception. Loss of *RluA-1* did
260 not have any impact on behavioral responses to gentle touch (**Figure 4B**) suggesting a
261 more specific involvement in nociception than for sensory processing in general.

262 **Expression pattern and nociception functions for RluA-2**

263 The *RluA-2* locus is adjacent to *RluA-1* on the second chromosome of *Drosophila*
264 *melanogaster*. *RluA-2* has significant sequence similarity with *RluA-1* within the
265 evolutionarily conserved pseudouridine synthase domain. This amino acid similarity of
266 *RluA1* and *RluA2* suggested possible functional overlap for the encoded proteins. To
267 investigate the expression of RluA-2 we generated a GFSTF line with RMCE of the *RluA-*
268 *2*^{MI12981} mimic element (**Figure S4A**) (Nagarkar-Jaiswal, DeLuca et al. 2015).
269 Immunostaining with anti-GFP labelled nuclei in all of the cell types that we observed in
270 third instar larvae (**Figure 5A**), including md neurons (**Figure 5B**).

271 To test the function of *RluA-2* we generated a deletion (*RluA-2*$^{del\text{-}HDR}$) to remove
272 its pseudouridine synthase domain via CRISPR/Cas9 HDR (**Figure S4A**). Also, since RluA-
273 1 and RluA-2 are both expressed in the md neurons (**Figure 1D** and **Figure 5B**), we
274 generated a double mutant (*RluA-1*$^{del\text{-}HDR}$*RluA-2*$^{del\text{-}HDR}$), by injecting the *RluA-2*$^{del\text{-}HDR}$
275 constructs in the *RluA-1*$^{del\text{-}HDR}$ null mutant background (**Figure S4**). The double mutant
276 allowed us to completely remove RluA pseudouridine synthase gene activity from the
277 flies. Prior to functional assessment, the single mutant and the double mutant were
278 backcrossed six times to the genetic background of iso*w*^{1118}.

279 We tested each single mutant (*RluA-1*$^{del\text{-}HDR}$ and *RluA-2*$^{del\text{-}HDR}$) together with the
280 double mutant *RluA-1*$^{del\text{-}HDR}$ *RluA-2*$^{del\text{-}HDR}$ side by side in thermal nociception assays with
281 the 42°C thermal stimulus. *RluA-1*$^{del\text{-}HDR}$ larvae (*RluA-1*$^{-/-}$) again responded significantly
282 faster than the genetic background control (**Figure 6**). The *RluA-2*$^{del\text{-}HDR}$ single mutant
283 larvae also displayed a faster response to the stimulus (**Figure 6**) and similar
284 hypersensitivity was also seen in an independent allele for *RluA-2* that we generated by
285 FLP/FRT mediated recombination (*RluA-2*$^{del\text{-}FRT}$) allele (**Figure S5**). Finally, the double
286 mutant *RluA-1*$^{del\text{-}HDR}$ *RluA-2*$^{del\text{-}HDR}$ larvae showed a faster response than the control larvae
287 (**Figure 6**) to the same extent as the single mutant of *RluA-2*$^{del\text{-}HDR}$. These results indicated
288 that *RluA-2*, like *RluA-1*, negatively regulates nociception. The finding that the double
289 mutant did not show a more severe phenotype than either single mutant suggests that
290 RluA-2 and RluA-1 have non-redundant functional roles, and that they may function in
291 the same molecular pathway. When this pathway is disrupted, hypersensitive nociception
292 results.

293 ***RluA-1* regulates neuronal dendrite morphology of nociceptors**

294 A nociceptor-specific RNAi screen with thermal nociception assay discovered
295 dozens of genes whose reduction caused either insensitive or hypersensitive thermal
296 nociception (Honjo, Mauthner et al. 2016). Interestingly, some of those genes targeted
297 with RNAi showed a reduced or increased branching of Class IV neuron dendrites.
298 Reduced dendrite branching was often seen with nociceptive insensitivity while
299 increased branching was found in some hypersensitive genotypes. Thus, regulation of

300 Class IV neuron dendrite morphology is a commonly affected developmental pathway
301 that is related to nociception phenotypes. Given this, we investigated the dendrite
302 morphology of the cIVda neuron dendrites in the *RluA-1*$^{del\text{-}HDR}$ mutant. In mutant ddaC
303 neurons visualized with *ppk-CD4-tdTom*ato, we observed a modest but significant
304 increase in the number of dendrite branches (normalized by neuron size) and shorter
305 average branch length in comparison to control animals (**Figures 7A and 7B**). We also
306 found that dendritic branches in the *RluA-1*$^{del\text{-}HDR}$ ddaC neurons had higher frequency of
307 isoneuronal cross-over events compared to the control (**Figures 7C and 7D**). This latter
308 phenotype is suggestive of an isoneuronal tiling defect. Increased isoneuronal crossovers
309 are also seen in mutants that affect dendrite attachment to the basal lamina (Han, Wang
310 et al. 2012, Kim, Coste et al. 2012, Meltzer, Yadav et al. 2016, Tenenbaum, Misra et al.
311 2017). Whether or not these dendrite abnormalities play a causal role in the
312 hypersensitive nociception phenotypes of the *RluA-1* mutant will be an interesting
313 subject for future investigation.

314 Materials and methods

315 Fly strains and husbandry

316 The following fly strains were obtained from Bloomington Stock Center: (*w*^{1118};
317 *PBac{vas-Cas9}VK00027*), *Mi{MIC}RluA-1*$^{[MI06897]}$, *Mi{MIC}RluA-2*$^{[MI12981]}$,
318 *Df(2L)Exel7048/CyO*, (*yw; Sp/CyO; pC-(lox-attB2-SA-T2A-Gal4-Hsp70)3*), (*yw hs-cre,*
319 *vasΦC31; Sp/CyO; Sb/TM3Ser*), (*P{ry=hsFLP}, yw M{vas-int.B}ZH-2A; Sp/CyO*; *P{FRT-*
320 *attB-{GFSTF}-attB(w+)-FRT}*), *ppk-CD4-tdTom*, *md-Gal4*, *UAS-mCD8::RFP*, *40XUAS-*

321 *mCD8::GFP*. The following fly strains were obtained from Exelixis collection at Harvard
322 Medical School: *PBac{WH}*^{f02750}, *P{XP}d2586*, *PBac{WH}Grip75*$^{[f05483]}$, *PBac{WH}RluA-2*$^{[f07702]}$.
323 The RNAi lines targeting *RluA-1* (31719-R1) were obtained from Kyoto Stock Center. The
324 genetic duplication line (BAC ID: CH321-49P21) covering *RluA-1* (starting at 24,819,420
325 and ending at 24,910,132 on 2R) was obtained from Genetivision. The nos-Cas9 line
326 used for generating *RluA-2*$^{del\text{-}HDR}$ and double mutant *RluA-1*$^{del\text{-}HDR}$*RluA-2*$^{del\text{-}HDR}$ [*y sc v; {nos-*
327 *Cas9} attP2* (TH00787.N)] was kindly provided by the Norbert Perrimon lab. All larvae
328 used in experiments were reared on the Bloomington *Drosophila* medium in an incubator
329 with controlled temperature (25°C) and humidity (70%) on a 12h light/12h dark cycle.
330 Strains were otherwise maintained at room temperature.

331 **CRIPSR targeting of *RluA-1* and *RluA-2***

332 HDR for mutagenesis used the CRISPR/Cas9 (Gratz et al. 2013) to generate *RluA-*
333 *1*$^{del\text{-}HDR}$, *RluA-2*$^{del\text{-}HDR}$ and the double mutant *RluA-1*$^{del\text{-}HDR}$*RluA-2*$^{del\text{-}HDR}$. Target sites were
334 selected using the flyCRISPR Optimal Target Finder. For the precise deletion of *RluA-1*,
335 the gRNA target sites are 5′ end 5′-CCACTG│TGCAGCGGAAAATTCAC-3′ (where "│"
336 represents the Cas9 cut site, which is 71bp upstream of the *RluA-1* transcriptional start)
337 and 3′ end: 5′-ACATATATTCAAAAGCT│CTTTGG-3′ (cut site at 60bp downstream of
338 *RluA-1* 3′UTR). We used the following primer pairs to amplify the 885bp *RluA-1*
339 homology ARM1: *RluA-1*-ARM1F: 5′-
340 AATACACCTGCATTATCGCTGGTCCCTGTGGCTTTGCAC-3′,

341 *RluA-1*-ARM1R: 5′-AATACACCTGCAATTCTACCAGTGGGGCAAACCGCATTT-3′. We
342 used *RluA-1*-ARM2F: 5′-GACTGCTCTTCGTATCTTTGGATGGTAAGTGCTTAAAC-3′
343 and *RluA-1*-ARM2R: 5′-ATTAGCTCTTCTGACCTTACAACTCCTTCAAGTCA-3′ to
344 amplify 969 bp of *RluA-1* homology ARM2. For *RluA-2*, we used a target site at the 5′
345 end: 5′-GCAATCTATAGGTCTGC│GGAAGC-3′ (cut site at bp 5 of exon 3) and at the 3′
346 end: 5′AAGATAAACTACAGAGA│CCCCGG-3′ (cutting site in the middle of exon 8) so
347 that the conserved pseudouridine synthase domain (located in exon 5) would be deleted.
348 Primer pairs *RluA-2*-ARM1F:
349 5'CTAACACCTGCATATTCGCTCGAAACCCATTGTTAGCTG3′ and *RluA-2* ARM1R: 5′
350 CATTCACCTGCATTACTACGCAGACCTATAGATTGCAAT3′ were used to amplify the
351 979bp *RluA-2* homology ARM1. *RluA-2*-ARM2F:
352 5′CAGTGCTCTTCGTATCCCCGGCACAAAGGATCTCA-3′, and *RluA-2*-ARM2R: 5′
353 GACTGCTCTTCCGACATTTCAATGCCCTTGGCCAA-3′ were used to amplify the RluA-
354 2 ARM2 (998bp). Rapid dsDNA donor cloning was carried out with the *pHD-DsRed-attP*
355 vector (Beumer and Carroll 2014) and the guide RNA (gRNAs) were cloned into *pU6-*
356 *BsbI-chiRNA* vector (Gratz, Cummings et al. 2013). Embryos of *vas-Cas9* on chromosome
357 III (w^{1118}; *PBac{y[+mDint2]=vas-Cas9}VK00027*, "injection line 1"*)* were injected with *RluA-*
358 *1* dsDNA donor and gRNAs to generate G_0 founders for *RluA-1*$^{del\text{-}HDR}$. Embryos with *nos-*
359 *Cas9* on chromosome III [*y sc v; {nos-Cas9} attP2* (TH00787.N), "injection line 2"] were
360 injected with *RluA-2* dsDNA donor and gRNAs to create the G_0 founders for *RluA-2*$^{del\text{-}}$
361 ^{HDR}. For generating the double mutant *RluA-1*$^{del\text{-}HDR}$*RluA-2*$^{del\text{-}HDR}$, *nos-Cas9* was first
362 introduced to the *RluA-1*$^{del\text{-}HDR}$ mutant background and the DsRed marker in *RluA-1*$^{del\text{-}HDR}$

363 removed with CRE recombinase and the resultant homozygous strain [*yw*; *RluA-1*$^{del-HDR}$*ΔDsRed*; *{nos-Cas9}attP2* (TH00787.N), "injection line 3"] was injected with the *RluA-*
364
365 *2* dsDNA donor and gRNAs. All embryo injections of the dsDNA donor (at a
366 concentration of 500ng/ul) and gRNAs (100ng/ul for each) were performed by the Model
367 system Injections (modelsysteminjections@flymsi.com).

368 To identify the desired HDR mutants, G_0 flies were crossed to w^{1118} and single F_1
369 founders were identified with DsRed fluorescence in the eyes (from *3XP3-DsRed* reporter)
370 and mated with a second chromosome balancer strain to establish independent lines.
371 Molecular testing for the desired events was performed by PCR on gDNA extracted from
372 candidates placed over a deficiency (*Df(2L)Exelixis7048*) covering the *RluA-1* and *RluA-2*
373 region (primer pairs marked in **Figures S2A** and **S4A, PCR amplication in Figure S2B**
374 **and S4B**). PCR products sequenced across the *attp-loxP-3XP3-DsRed-SV40-loxP*
375 fragment (**Figures S2C** and **Figures S4C**) confirmed accurate targeting of the loci. For
376 behavioral analysis, the original deletion mutants were backcrossed to *CS*, w^{1118} or
377 isow^{1118} for six times. For each generation, five heterozygous females were selected for
378 six successive backcrosses in vials and about 10 heterozygous females were used to cross
379 to a second chromosome balancer to produce balanced mutant males in bottles and
380 finally heterozygous mutant virgins and balanced males were crossed *en masse* in bottles
381 to establish the balanced and homozygous mutant lines. In all crosses the DsRed
382 fluorescence marker was used to follow the presence of the mutant.

383 **Generation of deletion line in *RluA-1* and *RluA-2* using FRT-mediated**
384 **deficiency**

385 FRT bearing insertions *{WH+}*^{f02750} and *{XP-}*^{d2586} and in *RluA-1* (locations marked
386 in **Figure S2A**) were used for generating a deficiency allele *RluA-1*$^{del\text{-}FRT}$. Insertions of
387 *{WH-}RluA-2*^{F07702} and *{WH-}Grip75*^{f05483} (locations marked in **Figure S4A**) were used for
388 generating the deficiency allele *RluA-2*$^{del\text{-}FRT}$. Crossing and heat-shock schemes followed
389 (Parks, Cook et al. 2004). Hybrid PCR with corresponding primers (WH5' plus / XP5'
390 minus left and right primers) was used to screen for candidate lines with *w-* deletion in
391 *RluA-1*$^{del\text{-}FRT}$ and two-sided PCR with left and right primers for WH3' minus/ WH5' minus
392 was used for screening for candidate lines with *w+* deletion in *RluA-2*$^{del\text{-}FRT}$ *(Parks, Cook*
393 *et al. 2004).* Molecular testing for the deletion was performed by PCR on gDNA
394 extracted from positive candidates placed over a deficiency (*Df(2L)Exelixis7048*) covering
395 the *RluA-1* and *RluA-2* region. The primers used for PCR and sequencing verification in
396 *RluA-1*$^{del\text{-}FRT}$ are *RluA-1-d2586*-up-F: 5'-AAAAATGCGGTTTGCCCC-3', located upstream
397 of the *{XP-}d2586* insertion site and *RluA-1-f02750*-down-R: 5'-
398 AAGGGGTAACAAAAGTCCAG-3', downstream of *{WH+}f02750 insertion site.*

399 **Generation of *RluA-1*^{GAL4} using "Trojan-exon"**

400 A triplet Trojan exon donor line on the 3rd chromosome *(yw; Sp/CyO; pC-(lox-*
401 *attB2-SA-T2A-Gal4-Hsp70)3)* and an *RluA-1* insertion line containing an intronic MiMIC
402 element (*Mi{MIC}RluA-1*$^{[MI06897]}$) were used to generate the *RluA-1*^{Gal4} driver using a
403 crossing scheme as described by (Diao, Ironfield et al. 2015). Candidate males who have

404 lost the y^+ selection marker associated with *MiMIC* were crossed to *40XUAS-mCD8::GFP*
405 line and animals expressing GFP were selected to establish a stable line. The line with
406 the correct linker (phase 0) was confirmed with sequencing of PCR products amplifying
407 the left side with primers *RluA-1*-5494F: 5′-TGATGTTGCCCCATAACG-3′ and *T2A-Gal4-*
408 Seq-1R: 5' CGCTATCGATGCTCACGGTC-3′ and the right side with the primers *T2A-*
409 *Gal4*-4F: 5'-ACACCGTGCTGATGCTGC-3′ and *RluA-1*-5907R: 5′-
410 GAAAACATCGCACATCTGG-3′ of the *RluA-1* genome-*T2A-Gal4* insertion bordering
411 region.

412 **Generation of GFSTF insertions in *RluA-1* and *RluA-2* by recombination**
413 **mediated cassette exchange (RMCE)**

414 Crossing, heat shocking and screening for EGFP tagged MiMIC lines in *RluA-1* and *RluA-*
415 *2* were essentially carried out as described (Nagarkar-Jaiswal, DeLuca et al. 2015). Males
416 carrying a MiMIC insertion in a coding intron of *RluA-1* (*RluA-1*^{MI06897}) or *RluA-2* (*RluA-*
417 *2*^{MI12981}) were crossed to females carrying the *hs-FLP* and *vasa-phiC31* integrase on the X
418 chromosome and a frame-specific ("phase 0") *FRT* flanked multiple tag (*GFSTF*) cassette
419 on chromosome III. Candidate males with mosaic *w-* eyes and *y-* bodies were individually
420 crossed to *w; Sco/CyO; Sb/TM3 Ser* balancers to establish stocks. The presence and
421 direction of the insertion were tested by PCR assays described (Venken, Schulze et al.
422 2011). Since the original MiMIC insertion in *RluA-1* or *RluA-2* and the respective gene
423 are in the same orientation, positive PCR reaction 1 (with primers MiLF and TagR) and 4

424 (with primers MilR and TagF) as described (Venken, Schulze et al. 2011) indicated a
425 successful RMCE event and resulted in expression.

426 **Generation of *UAS-RluA-1***

427 *Drosophila RluA-1* full length cDNA clone for *RluA-1* transcript A (FI04540) was
428 obtained from the Drosophila Genome Resource Center (DGRC). The *UAS-RluA-1*
429 expression constructs were generated with the ENTR/gateway system following the
430 instructions of the manufacturer (Invitrogen). The *RluA-1*-cDNA-F (5'-
431 CACCATGCAGAATTCTCCGGCT-3', and *RluA-1*-cDNA+STOP-R (5'-
432 TCATGCCGAGTCTAAGTG-3' primers were used to amplify the open reading frame and
433 cloned into *pENTR-D-TOPO* vector. The sequence was verified and then cloned to the
434 P-element based destination vector *pTW*. Model System Injections performed injections
435 into w^{1118} embryos. F_0 flies were crossed to w^{1118} and single F_1 founders were identified
436 based on the w^+ marker. Individual lines were mapped and balanced to establish stable
437 stocks. A *UAS-RluA-1* line with relatively weak expression evaluated by Q-PCR in *RluA-*
438 *1*-cDNA lines driven by *md-GAL4* was used for the cIV-neuron specific *RluA-1*-cDNA
439 rescue experiment (**Figure 3B**).

440 **Larval behavioral analyses**

441 Wandering 3rd instar larvae were washed out from vials and acclimated for 5 min in petri
442 dishes before testing. Larval thermal nociception assays were conducted essentially as
443 previously described (Caldwell and Tracey 2010, Mauthner, Hwang et al. 2014, Walcott,
444 Mauthner et al. 2018), except that the probe is gently held against the lateral surface of

445 abdominal segments 4, 5, or 6 until the animal completes a 360° roll along the dorsal-
446 ventral axis. All animals tested eventually performed rolling and the response latency
447 from all the animals was graphed for a given genotype. Larval mechanical nociception
448 response assays were conducted as previously described (Mauthner, Hwang et al. 2014).
449 Behavioral recording and scoring were performed with the observer blinded to the
450 genotype.

451 For gentle touch assays, early L3 larvae were scooped out from the top layer of
452 the fly food in the vials and 5-10 larvae were briefly rinsed with PBS and allowed to
453 acclimate on 1% agarose in a plate for 5 min before testing with an eyelash fixed to the
454 end of a paintbrush. Each larva was brushed with the eyelash on segments T1-A3 for 4
455 times and the responses were recorded and summarized using a gentle touch scale
456 (Tsubouchi, Caldwell et al. 2012).

457 **Immunohistochemistry and microscopy**

458 The following primary antibodies were used for immunofluorescence: rabbit anti-GFP
459 (ab6556, Abcam, 1:500), mouse anti-GFP (ab38689, Abcam, 1:500), Rabbit anti-HRP
460 (1:100), mouse anti-nc82 (DSHB, supernatant, 1:30). Alexa Fluor 488, 633 were used at
461 1:1000 as secondary antibodies. Detailed immunostaining protocol is available on
462 request. Images for immunostained tissues were taken on a Zeiss LSM 5 LIVE confocal
463 microscope using a 40X objective except for **Figure 1D** and **Figure S1B**, which were
464 taken on a Zeiss LSM880 using the 63X objective.

465 **CIV dendrite imaging, tracing and analysis**

466 To image class IV dendrites, the DsRed marker in *RluA-1*$^{del\text{-}HDR}$ was first removed with
467 CRE recombinase (*w*^{1118}*; RluA-1*$^{del\text{-}HDR\Delta DsRed}$) and *ppk1.9-CD4::tdTom* was introduced to
468 the mutant background and a stable homozygous stock was established. For CIV
469 dendrite analysis, six virgins and three males were crossed in each vial for the mutant
470 (*w*^{1118}; *RluA-1*$^{del\text{-}HDR\Delta DsRed}$*; ppk1.9-CD4::tdTom*) and control (*ppk1.9-CD4::-td-Tom*).
471 Wandering larvae were anesthetized with diethyl ether in a sealed glass chamber for
472 15min before being arranged on a slide and covered with 50 mm glass coverslip.
473 Neurons expressing the fluorescently tagged markers were visualized on a Zeiss LSM 5
474 Live confocal microscope with a 40X oil objective (Plan Apo M27, NA 0.8). Images were
475 collected as 5x3 tiles scans of z-stacks with 512x512 resolution. A MatLab build was used
476 for initial automatic tracing of the ddaC neuron dendrites from the confocal z-stack
477 series TIFF images (Gulyanon 2016). The generated SWC files were overlaid onto the
478 maximum intensity projected image of the neuron in neuTube (Feng, Zhao et al.
479 2015) and manually curated to eliminate tracing errors made by MatLab. The corrected
480 images were then analyzed with MatLab to extract neuron features of interest including
481 number of branches, average branch length, and neuron size (the estimated size of the
482 neuron, defined as the area of the minimum bounding circle) (Gulyanon 2016). Iso-
483 neuronal crossover events were quantified manually from the traced dendrites for each
484 genotype (n=6 neurons).

485 **Statistical analysis**

486 Statistics were performed using GraphPad Prism 4. Thermal and gentle touch behavioral
487 data were compared with an unpaired non-parametric Mann-Whitney test when
488 comparing two groups and Kruskal-Wallis test when comparing three or more groups.
489 Mechanical nociception behavioral data were compared with Fisher's exact test.
490 Dendrite morphology data were compared with the Student's t test. Error bars represent
491 S.D. in all the figures unless otherwise specified.

492 **Data and Reagent Availability Statement**

493 Strains and plasmids are available upon request. All supplementary figures have been
494 uploaded to figshare. The authors affirm that all data necessary for confirming the
495 conclusions of the article are present within the article and its figures.

496 Discussion

497 Given the well-established nociceptive role of md-neurons, we have investigated
498 the historically first known molecular marker for md-neurons in nociception pathways.
499 This gene encodes the RluA-1 protein in the RluA family of pseudouridine synthases. Our
500 studies clearly demonstrate that loss of function for either *RluA-1* or *RluA-2* produce
501 hyperalgesia in third instar *Drosophila* larvae. Tissue-specific RNAi, genetic null mutant,
502 and cDNA rescue experiments all indicate that loss of the *RluA-1* gene from whole
503 animals, or specifically from nociceptors, results in hyperalgesia. A newly generated
504 *RluA-1*^{GAL4} driver showed specific expression in larval multidendritic and ES neurons. As
505 well, a GFP exon trap for RluA-1 protein localized to the nuclei of these neurons. A small
506 number of unidentified neurons in the larval brain were also revealed by *RluA-1*^{GAL4} and

507 we observed expression of *RluA-1*^{GAL4} driven mCD8GFP and GFP tagged RluA-1 in cells
508 of the adult brain, which included the optic lobe.

509 Although loss of *RluA-2* also caused hyperalgesia, its expression pattern was
510 ubiquitous and included multidendritic neurons. Like the RluA-1 GFP exon trap, the
511 RluA-2 GFP exon trap labelled nuclei. The nuclear localization for both RluA-1 and RluA-
512 2 may indicate that these proteins act on RNA targets prior to export of the nucleus, or
513 that they predominantly act upon nuclear localized RNAs. A caveat to this interpretation
514 is that we have yet to demonstrate that these molecules function as genuine
515 pseudouridine synthases, and this function remains a hypothesis that is based on the
516 known function of evolutionary homologues. This hypothetical function requires future
517 biochemical verification.

518 We also observed that *RluA-1* mutants showed an increase in the number of
519 dendrite branches relative to control genotypes as well as an increase in isoneuronal
520 crossovers. Transcription factors, cytoskeletal regulators, motor proteins, secretory
521 pathways and cell adhesion molecules all function in concert to develop and maintain
522 optimum dendrite morphology (Corty, Matthews et al. 2009). RluA-1 may modify RNAs
523 for those genes that regulate dendritic morphology, or changes in the dendrite
524 morphology could be an indirect consequence of neuronal sensitivity that is regulated
525 by RluA-1. It is noteworthy that prior studies have noted a potential link between the
526 degree of dendrite branching and the sensitivity of nociception behaviors (Honjo,
527 Mauthner et al. 2016). In other cases, axonal factors such as the ion channel SK have
528 been found to be important in regulating the cIVda neuron excitability (Onodera, Baba

529 et al. 2017, Walcott, Mauthner et al. 2018). Whether the dendrite branching phenotype
530 that we observe in *RluA-1* mutants is a cause or a consequence of hypersensitivity will be
531 an interesting question for future studies.

532 A large body of literature indicates that RNA trafficking and local translation is
533 important in dendrites and axons of neurons (Glock, Heumuller et al. 2017, Rangaraju,
534 Tom Dieck et al. 2017). Relative to uridine the pseudourine base is believed to have
535 enhanced rotational freedom which may alter conformation of RNA secondary structures.
536 As well, an additional hydrogen bond donor present in pseudouridine may favor
537 alternative base-pairing interactions in RNA. These properties may consequently alter
538 RNA localization, stability and/or efficiency of translation (Arnez and Steitz 1994, Newby
539 and Greenbaum 2002, Kariko, Muramatsu et al. 2008). Pseudouridines can also influence
540 decoding during translation as pseudouridylation of nonsense codons has been shown
541 to suppress translation termination both *in vitro* and *in vivo* (Karijolich and Yu 2011). Thus,
542 another possible function for pseudouridylation in nociceptive neurons could be to favor
543 read-through of pseudouridylated stop codons to generate novel sequences at protein
544 carboxy termini.

545 The precise mechanism explaining the involvement of RluA proteins in
546 nociception can only be elucidated by identifying the RNA targets of these enzymes.
547 Several groups have developed methods using next generation sequencing methods to
548 identify the pseudouridine sites in transcriptomes (Carlile, Rojas-Duran et al. 2014,
549 Lovejoy, Riordan et al. 2014, Schwartz, Bernstein et al. 2014, Li, Zhu et al. 2015,
550 Khoddami, Yerra et al. 2019). Future investigations applying these methods to wild type

551 and *RluA* mutants in *Drosophila* will help us to identify the RluA targets and to further
552 define the underlying mechanisms.
553

554 Acknowledgements

555 The authors thank Drosophila Genomic Resource Center (supported by NIH grant
556 2P40OD010949) for clones. Stocks obtained from the Bloomington Drosophila Stock
557 Center (NIH P40OD018537) were used in this study. We also thank the KYOTO Stock
558 Center Kyoto in Kyoto Institute of Technology and Harvard Medical School for providing
559 fly stocks used in this study. Members of Tracey lab provided helpful feedback on the
560 manuscript and Jayce Brown Culbertson assisted with dendrite tracing.

561 References

562 Ainsley, J. A., J. M. Pettus, D. Bosenko, C. E. Gerstein, N. Zinkevich, M. G. Anderson, C.
563 M. Adams, M. J. Welsh and W. A. Johnson (2003). "Enhanced locomotion caused by loss
564 of the Drosophila DEG/ENaC protein Pickpocket1." Curr Biol **13**(17): 1557-1563.

565 Arnez, J. G. and T. A. Steitz (1994). "Crystal structure of unmodified tRNA(Gln)
566 complexed with glutaminyl-tRNA synthetase and ATP suggests a possible role for
567 pseudo-uridines in stabilization of RNA structure." Biochemistry **33**(24): 7560-7567.

568 Beumer, K. J. and D. Carroll (2014). "Targeted genome engineering techniques in
569 Drosophila." Methods **68**(1): 29-37.

570 Bianco, A., M. Dienstbier, H. K. Salter, G. Gatto and S. L. Bullock (2010). "Bicaudal-D
571 regulates fragile X mental retardation protein levels, motility, and function during
572 neuronal morphogenesis." Curr Biol **20**(16): 1487-1492.

573 Brechbiel, J. L. and E. R. Gavis (2008). "Spatial regulation of nanos is required for its
574 function in dendrite morphogenesis." Curr Biol **18**(10): 745-750.

575 Brewster, R. and R. Bodmer (1995). "Origin and specification of type II sensory neurons
576 in Drosophila." Development **121**(9): 2923-2936.

577 Burgos, A., K. Honjo, T. Ohyama, C. S. Qian, G. J. Shin, D. M. Gohl, M. Silies, W. D.
578 Tracey, M. Zlatic, A. Cardona and W. B. Grueber (2018). "Nociceptive interneurons
579 control modular motor pathways to promote escape behavior in Drosophila." Elife **7**.

580 Caldwell, J. C. and W. D. Tracey (2010). "Alternatives to Mammalian Pain Models 2:
581 Using Drosophila to Identify Novel Genes Involved in Nociception." Analgesia: Methods
582 and Protocols **617**: 19-29.

583 Carlile, T. M., M. F. Rojas-Duran, B. Zinshteyn, H. Shin, K. M. Bartoli and W. V. Gilbert
584 (2014). "Pseudouridine profiling reveals regulated mRNA pseudouridylation in yeast and
585 human cells." Nature **515**(7525): 143-+.

586 Chin, M. R. and W. D. Tracey, Jr. (2017). "Nociceptive Circuits: Can't Escape Detection."
587 Curr Biol **27**(16): R796-R798.

588 Corty, M. M., B. J. Matthews and W. B. Grueber (2009). "Molecules and mechanisms of
589 dendrite development in Drosophila." Development **136**(7): 1049-1061.

590 de Brouwer, A. P. M., R. Abou Jamra, N. Kortel, C. Soyris, D. L. Polla, M. Safra, A. Zisso,
591 C. A. Powell, P. Rebelo-Guiomar, N. Dinges, V. Morin, M. Stock, M. Hussain, M. Shahzad,
592 S. Riazuddin, Z. M. Ahmed, R. Pfundt, F. Schwarz, L. de Boer, A. Reis, D. Grozeva, F. L.
593 Raymond, S. Riazuddin, D. A. Koolen, M. Minczuk, J. Y. Roignant, H. van Bokhoven and
594 S. Schwartz (2018). "Variants in PUS7 Cause Intellectual Disability with Speech Delay,
595 Microcephaly, Short Stature, and Aggressive Behavior." Am J Hum Genet **103**(6): 1045-
596 1052.

597 Diao, F., H. Ironfield, H. Luan, F. Diao, W. C. Shropshire, J. Ewer, E. Marr, C. J. Potter,
598 M. Landgraf and B. H. White (2015). "Plug-and-play genetic access to drosophila cell
599 types using exchangeable exon cassettes." Cell reports **10**(8): 1410-1421.

600 Feng, L., T. Zhao and J. Kim (2015). "neuTube 1.0: A New Design for Efficient Neuron
601 Reconstruction Software Based on the SWC Format." eNeuro **2**(1).

602 Fujiwara, T. and H. Harigae (2013). "Pathophysiology and genetic mutations in
603 congenital sideroblastic anemia." Pediatrics International **55**(6): 675-679.

604 Gaskin, D. J. and P. Richard (2012). "The economic costs of pain in the United States." J
605 Pain **13**(8): 715-724.

606 Ge, J. and Y. T. Yu (2013). "RNA pseudouridylation: new insights into an old
607 modification." Trends Biochem Sci **38**(4): 210-218.

608 Giordano, E., I. Peluso, S. Senger and M. Furia (1999). "minifly, a Drosophila gene
609 required for ribosome biogenesis." J Cell Biol **144**(6): 1123-1133.

610 Glock, C., M. Heumuller and E. M. Schuman (2017). "mRNA transport & local translation
611 in neurons." Curr Opin Neurobiol **45**: 169-177.

612 Gorczyca, D. A., S. Younger, S. Meltzer, S. E. Kim, L. Cheng, W. Song, H. Y. Lee, L. Y.
613 Jan and Y. N. Jan (2014). "Identification of Ppk26, a DEG/ENaC Channel Functioning
614 with Ppk1 in a Mutually Dependent Manner to Guide Locomotion Behavior in
615 Drosophila." Cell Rep **9**(4): 1446-1458.

616 Gratz, S. J., A. M. Cummings, J. N. Nguyen, D. C. Hamm, L. K. Donohue, M. M. Harrison,
617 J. Wildonger and K. M. O'Connor-Giles (2013). "Genome engineering of Drosophila with
618 the CRISPR RNA-guided Cas9 nuclease." Genetics **194**(4): 1029-1035.

619 Grueber, W. B., L. Y. Jan and Y. N. Jan (2002). "Tiling of the Drosophila epidermis by
620 multidendritic sensory neurons." Development **129**(12): 2867-2878.

621 Gulyanon, S., Sharifai, N., Kim, M. D., Chiba, A., Tsechpenakis, G. (2016). CRF
622 formulation of active contour population for efficient three-dimensional neurite tracing.
623 2016 IEEE 13th International Symposium on Biomedical Imaging**:** 593-597.

624 Gutgsell, N. S., M. P. Deutscher and J. Ofengand (2005). "The pseudouridine synthase
625 RluD is required for normal ribosome assembly and function in Escherichia coli." Rna-a
626 Publication of the Rna Society **11**(7): 1141-1152.

627 Hammal, T. and A. R. Ferre-D'Amare (2006). "Pseudouridine synthases." Chemistry &
628 Biology **13**(11): 1125-1135.

629 Han, C., D. Wang, P. Soba, S. Zhu, X. Lin, L. Y. Jan and Y. N. Jan (2012). "Integrins
630 regulate repulsion-mediated dendritic patterning of drosophila sensory neurons by
631 restricting dendrites in a 2D space." Neuron **73**(1): 64-78.

632 Hoang, C., J. J. Chen, C. A. Vizthum, J. M. Kandel, C. S. Hamilton, E. G. Mueller and A.
633 R. Ferre-D'Amare (2006). "Crystal structure of pseudouridine synthase RluA: Indirect
634 sequence readout through protein-induced RNA structure." Molecular Cell **24**(4): 535-
635 545.

636 Honjo, K., S. E. Mauthner, Y. Wang, J. H. Skene and W. D. Tracey, Jr. (2016).
637 "Nociceptor-Enriched Genes Required for Normal Thermal Nociception." Cell Rep
638 **16**(2): 295-303.

639 Hu, C., M. Petersen, N. Hoyer, B. Spitzweck, F. Tenedini, D. Wang, A. Gruschka, L. S.
640 Burchardt, E. Szpotowicz, M. Schweizer, A. R. Guntur, C. H. Yang and P. Soba (2017).
641 "Sensory integration and neuromodulatory feedback facilitate Drosophila
642 mechanonociceptive behavior." Nat Neurosci **20**(8): 1085-1095.

643 Hwang, R. Y., L. Zhong, Y. Xu, T. Johnson, F. Zhang, K. Deisseroth and W. D. Tracey
644 (2007). "Nociceptive neurons protect Drosophila larvae from parasitoid wasps." Curr Biol
645 **17**(24): 2105-2116.

646 Im, S. H. and M. J. Galko (2012). "Pokes, sunburn, and hot sauce: Drosophila as an
647 emerging model for the biology of nociception." Developmental Dynamics **241**(1): 16-
648 26.

649 Karijolich, J. and Y. T. Yu (2011). "Converting nonsense codons into sense codons by
650 targeted pseudouridylation." Nature **474**(7351): 395-+.

651 Kariko, K., H. Muramatsu, F. A. Welsh, J. Ludwig, H. Kato, S. Akira and D. Weissman
652 (2008). "Incorporation of pseudouridine into mRNA yields superior nonimmunogenic
653 vector with increased translational capacity and biological stability." Mol Ther **16**(11):
654 1833-1840.

655 Khoddami, V., A. Yerra, T. L. Mosbruger, A. M. Fleming, C. J. Burrows and B. R. Cairns
656 (2019). "Transcriptome-wide profiling of multiple RNA modifications simultaneously at
657 single-base resolution." Proc Natl Acad Sci U S A **116**(14): 6784-6789.

658 Khuong, T. M., Q. P. Wang, J. Manion, L. J. Oyston, M. T. Lau, H. Towler, Y. Q. Lin and
659 G. G. Neely (2019). "Nerve injury drives a heightened state of vigilance and neuropathic
660 sensitization in Drosophila." Sci Adv **5**(7): eaaw4099.

661 Kim, S. E., B. Coste, A. Chadha, B. Cook and A. Patapoutian (2012). "The role of
662 Drosophila Piezo in mechanical nociception." Nature **483**(7388): 209-212.

663 Knight, S. W., N. S. Heiss, T. J. Vulliamy, S. Greschner, G. Stavrides, G. S. Pai, G.
664 Lestringant, N. Varma, P. J. Mason, I. Dokal and A. Poustka (1999). "X-linked dyskeratosis
665 congenita is predominantly caused by missense mutations in the DKC1 gene." American
666 Journal of Human Genetics **65**(1): 50-58.

667 Koonin, E. V. (1996). "Pseudouridine synthases: four families of enzymes containing a
668 putative uridine-binding motif also conserved in dUTPases and dCTP deaminases."
669 Nucleic Acids Res **24**(12): 2411-2415.

670 Li, X. Y., P. Zhu, S. Q. Ma, J. H. Song, J. Y. Bai, F. F. Sun and C. Q. Yi (2015). "Chemical
671 pulldown reveals dynamic pseudouridylation of the mammalian transcriptome." Nature
672 Chemical Biology **11**(8): 592-U593.

673 Lovejoy, A. F., D. P. Riordan and P. O. Brown (2014). "Transcriptome-Wide Mapping of
674 Pseudouridines: Pseudouridine Synthases Modify Specific mRNAs in S. cerevisiae." Plos
675 One **9**(10).

676 Mauthner, S. E., R. Y. Hwang, A. H. Lewis, Q. Xiao, A. Tsubouchi, Y. Wang, K. Honjo, J.
677 H. P. Skene, J. Grandl and W. D. Tracey (2014). "Balboa Binds to Pickpocket In Vivo and
678 Is Required for Mechanical Nociception in Drosophila Larvae." Current Biology **24**(24).

679 Meltzer, S., S. Yadav, J. Lee, P. Soba, S. H. Younger, P. Jin, W. Zhang, J. Parrish, L. Y.
680 Jan and Y. N. Jan (2016). "Epidermis-Derived Semaphorin Promotes Dendrite Self-
681 Avoidance by Regulating Dendrite-Substrate Adhesion in Drosophila Sensory Neurons."
682 Neuron **89**(4): 741-755.

683 Milinkeviciute, G., C. Gentile and G. G. Neely (2012). "Drosophila as a tool for studying
684 the conserved genetics of pain." Clinical Genetics **82**(4): 359-366.

685 Nagarkar-Jaiswal, S., S. Z. DeLuca, P.-T. Lee, W.-W. Lin, H. Pan, Z. Zuo, J. Lv, A. C.
686 Spradling and H. J. Bellen (2015). "A genetic toolkit for tagging intronic MiMIC
687 containing genes." eLife **4**.

688 Neely, G. G., A. Hess, M. Costigan, A. C. Keene, S. Goulas, M. Langeslag, R. S. Griffin, I.
689 Belfer, F. Dai, S. B. Smith, L. Diatchenko, V. Gupta, C. P. Xia, S. Amann, S. Kreitz, C.
690 Heindl-Erdmann, S. Wolz, C. V. Ly, S. Arora, R. Sarangi, D. Dan, M. Novatchkova, M.
691 Rosenzweig, D. G. Gibson, D. Truong, D. Schramek, T. Zoranovic, S. J. Cronin, B. Angjeli,
692 K. Brune, G. Dietzl, W. Maixner, A. Meixner, W. Thomas, J. A. Pospisilik, M. Alenius, M.
693 Kress, S. Subramaniam, P. A. Garrity, H. J. Bellen, C. J. Woolf and J. M. Penninger (2010).
694 "A genome-wide Drosophila screen for heat nociception identifies alpha2delta3 as an
695 evolutionarily conserved pain gene." Cell **143**(4): 628-638.

696 Newby, M. I. and N. L. Greenbaum (2002). "Sculpting of the spliceosomal branch site
697 recognition motif by a conserved pseudouridine." Nature Structural Biology **9**(12): 958-
698 965.

699 Ohyama, T., T. Jovanic, G. Denisov, T. C. Dang, D. Hoffmann, R. A. Kerr and M. Zlatic
700 (2013). "High-throughput analysis of stimulus-evoked behaviors in Drosophila larva
701 reveals multiple modality-specific escape strategies." PLoS One **8**(8): e71706.

702 Ohyama, T., C. M. Schneider-Mizell, R. D. Fetter, J. V. Aleman, R. Franconville, M. Rivera-
703 Alba, B. D. Mensh, K. M. Branson, J. H. Simpson, J. W. Truman, A. Cardona and M. Zlatic
704 (2015). "A multilevel multimodal circuit enhances action selection in Drosophila." Nature
705 **520**(7549): 633-639.

706 Olesnicky, E. C., D. J. Killian, E. Garcia, M. C. Morton, A. R. Rathjen, I. E. Sola and E. R.
707 Gavis (2014). "Extensive use of RNA-binding proteins in Drosophila sensory neuron
708 dendrite morphogenesis." G3 (Bethesda) **4**(2): 297-306.

709 Onodera, K., S. Baba, A. Murakami, T. Uemura and T. Usui (2017). "Small conductance
710 Ca(2+)-activated K(+) channels induce the firing pause periods during the activation of
711 Drosophila nociceptive neurons." Elife **6**.

712 Pan, L., Y. Q. Zhang, E. Woodruff and K. Broadie (2004). "The Drosophila fragile X gene
713 negatively regulates neuronal elaboration and synaptic differentiation." Curr Biol **14**(20):
714 1863-1870.

715 Parks, A. L., K. R. Cook, M. Belvin, N. A. Dompe, R. Fawcett, K. Huppert, L. R. Tan, C. G.
716 Winter, K. P. Bogart, J. E. Deal, M. E. Deal-Herr, D. Grant, M. Marcinko, W. Y. Miyazaki,
717 S. Robertson, K. J. Shaw, M. Tabios, V. Vysotskaia, L. Zhao, R. S. Andrade, K. A. Edgar,
718 E. Howie, K. Killpack, B. Milash, A. Norton, D. Thao, K. Whittaker, M. A. Winner, L.
719 Friedman, J. Margolis, M. A. Singer, C. Kopczynski, D. Curtis, T. C. Kaufman, G. D.
720 Plowman, G. Duyk and H. L. Francis-Lang (2004). "Systematic generation of high-
721 resolution deletion coverage of the Drosophila melanogaster genome." Nat Genet
722 **36**(3): 288-292.

723 Phillips, B., A. N. Billin, C. Cadwell, R. Buchholz, C. Erickson, J. R. Merriam, J. Carbon
724 and S. J. Poole (1998). "The Nop60B gene of Drosophila encodes an essential nucleolar
725 protein that functions in yeast." Mol Gen Genet **260**(1): 20-29.

726 Ran, F. A., P. D. Hsu, J. Wright, V. Agarwala, D. A. Scott and F. Zhang (2013). "Genome
727 engineering using the CRISPR-Cas9 system." Nat Protoc **8**(11): 2281-2308.

728 Rangaraju, V., S. Tom Dieck and E. M. Schuman (2017). "Local translation in neuronal
729 compartments: how local is local?" EMBO Rep **18**(5): 693-711.

730 Raychaudhuri, S., L. Niu, J. Conrad, B. G. Lane and J. Ofengand (1999). "Functional effect
731 of deletion and mutation of the Escherichia coli ribosomal RNA and tRNA pseudouridine
732 synthase RluA." J Biol Chem **274**(27): 18880-18886.

733 Schwartz, S., D. A. Bernstein, M. R. Mumbach, M. Jovanovic, R. H. Herbst, B. X. Leon-
734 Ricardo, J. M. Engreitz, M. Guttman, R. Satija, E. S. Lander, G. Fink and A. Regev (2014).
735 "Transcriptome-wide mapping reveals widespread dynamic-regulated
736 pseudouridylation of ncRNA and mRNA." Cell **159**(1): 148-162.

737 Tenenbaum, C. M., M. Misra, R. A. Alizzi and E. R. Gavis (2017). "Enclosure of Dendrites
738 by Epidermal Cells Restricts Branching and Permits Coordinated Development of
739 Spatially Overlapping Sensory Neurons." Cell Rep **20**(13): 3043-3056.

740 Tracey, W. D., Jr. (2017). "Nociception." Curr Biol **27**(4): R129-R133.

741 Tracey, W. D., R. I. Wilson, G. Laurent and S. Benzer (2003). "painless, a Drosophila gene
742 essential for nociception." Cell **113**(2): 261-273.

743 Tsubouchi, A., J. C. Caldwell and W. D. Tracey (2012). "Dendritic filopodia, Ripped
744 Pocket, NOMPC, and NMDARs contribute to the sense of touch in Drosophila larvae."
745 Curr Biol **22**(22): 2124-2134.

746 Turner, H. N., K. Armengol, A. A. Patel, N. J. Himmel, L. Sullivan, S. C. Iyer, S.
747 Bhattacharya, E. P. R. Iyer, C. Landry, M. J. Galko and D. N. Cox (2016). "The TRP
748 Channels Pkd2, NompC, and Trpm Act in Cold-Sensing Neurons to Mediate Unique
749 Aversive Behaviors to Noxious Cold in Drosophila." Curr Biol **26**(23): 3116-3128.

750 Venken, K. J., J. W. Carlson, K. L. Schulze, H. Pan, Y. He, R. Spokony, K. H. Wan, M.
751 Koriabine, P. J. de Jong, K. P. White, H. J. Bellen and R. A. Hoskins (2009). "Versatile
752 P[acman] BAC libraries for transgenesis studies in Drosophila melanogaster." Nat
753 Methods **6**(6): 431-434.

754 Venken, K. J. T., K. L. Schulze, N. A. Haelterman, H. Pan, Y. He, M. Evans-Holm, J. W.
755 Carlson, R. W. Levis, A. C. Spradling, R. A. Hoskins and H. J. Bellen (2011). "MiMIC: a
756 highly versatile transposon insertion resource for engineering Drosophila melanogaster
757 genes." Nature methods **8**(9): 737-743.

758 Vicidomini, R., A. Petrizzo, A. di Giovanni, L. Cassese, A. A. Lombardi, C. Pragliola and
759 M. Furia (2017). "Drosophila dyskerin is required for somatic stem cell homeostasis." Sci
760 Rep **7**(1): 347.

761 Walcott, K. C. E., S. E. Mauthner, A. Tsubouchi, J. Robertson and W. D. Tracey (2018).
762 "The Drosophila Small Conductance Calcium-Activated Potassium Channel Negatively
763 Regulates Nociception." Cell Rep **24**(12): 3125-3132 e3123.

764 Wang, C. C., J. C. Lo, C. T. Chien and M. L. Huang (2011). "Spatially controlled
765 expression of the Drosophila pseudouridine synthase RluA-1." Int J Dev Biol **55**(2): 223-
766 227.

767 Xiang, Y., Q. Yuan, N. Vogt, L. L. Looger, L. Y. Jan and Y. N. Jan (2010). "Light-avoidance-
768 mediating photoreceptors tile the Drosophila larval body wall." Nature **468**(7326): 921-
769 926.

770 Xu, X., J. L. Brechbiel and E. R. Gavis (2013). "Dynein-dependent transport of nanos RNA
771 in Drosophila sensory neurons requires Rumpelstiltskin and the germ plasm organizer
772 Oskar." J Neurosci **33**(37): 14791-14800.

773 Ye, B., C. Petritsch, I. E. Clark, E. R. Gavis, L. Y. Jan and Y. N. Jan (2004). "Nanos and
774 Pumilio are essential for dendrite morphogenesis in Drosophila peripheral neurons."
775 Curr Biol **14**(4): 314-321.

776 Zhong, L., A. Bellemer, H. Yan, H. Ken, R. Jessica, R. Y. Hwang, G. S. Pitt and W. D.
777 Tracey (2012). "Thermosensory and nonthermosensory isoforms of Drosophila

778 melanogaster TRPA1 reveal heat-sensor domains of a thermoTRP Channel." Cell Rep
779 **1**(1): 43-55.

780 Zhong, L., R. Y. Hwang and W. D. Tracey (2010). "Pickpocket is a DEG/ENaC protein
781 required for mechanical nociception in Drosophila larvae." Curr Biol **20**(5): 429-434.

782 ## Figure Legends

783 **Figure 1**. ***RluA-1* gene and protein expression in *Drosophila melanogaster*.** (**A**) A low
784 magnification confocal micrograph of *RluA-1* gene expression pattern in the larval PNS
785 (third instar w^{1118}; *RluA-1*^{Gal4}/*40xUAS-mCD8::GFP*). Note that GFP positive signals are
786 detected in peripheral sensory neurons in each segment along the larval body wall. Scale
787 bar=500μm. (**B**) Higher magnification of an abdominal dorsal PNS cluster. *RluA-1*^{Gal4} is
788 expressed in the cell body and dendrites of all classes of multidendritic neurons, external
789 sensory (ES), dorsal multiple dendrite neuron (dmd1) and dorsal bipolar dendritic (dbd)
790 neurons (ddaD and ddaE (Class I), ddaB (Class II), ddaA and ddaF (Class III), and ddaC
791 (ClassIV), ES, dmd1 and dbd neurons are labeled). Scale bar = 50μm. (**C**). *RluA-1*^{Gal4}*/+*
792 driving expression of *40xUAS-mCD8::GFP/+* in the larval CNS. Labelling is observed in
793 axonal projections of sensory neurons in the larval ventral nerve cord and unidentified
794 clusters of neurons in the larval brain. Scale bar =5 0μm. (**D**$^{1-3}$) anti-GFP
795 immunohistochemistry of a third instar larval fillet preparation of *RluA-1-GFSTF/*
796 *Gal4109(2)80>UAS-mCD8-RFP*, immunoreactive signals are detected in the nuclei of
797 multi-dendritic neurons (D^1 green, GFP) surrounded by the membrane-localized RFP
798 signal (D^2 magenta, RFP) and merged image in D^3. Scale bar = 50μm.

799 **Figure 2. Thermal nociception in animals with *RluA-1* loss of function. (A).** Class IV
800 specific knock-down in *RluA-1* results in significant hypersensitive thermal nociception in

801 larvae compared to the *ppk-GAL4* driver alone animals at 46°C (average latency of 1.33
802 ± 1.10 sec for *ppk-Gal4* > *UAS-RluA-1-RNAi (*31719-R1*)*, n=38 vs. 2.04 ± 1.89 sec for *ppk-*
803 *GAL4* driver alone, n=37. P<0.05), albeit not statistically significant compared to the
804 UAS-RNAi alone (1.96 ± 1.32 sec for UAS-RNAi alone, n=27). These differences are more
805 pronounced at 42°C (average latency of 1.92 ± 1.16 sec for *ppk-Gal4* > *UAS-RluA-1-*
806 *RNAi*, n=35 vs. 6.25 ± 2.51 sec for *ppk-GAL4* driver alone controls, n=42 or 5.20 ± 3.28
807 sec for UAS-RNAi alone controls, n=49, P<0.0001). Kruskal-Wallis test with Dunn's
808 multiple comparison tests, only significant comparisons were labeled. **(B).** Homozygous
809 null mutant *RluA-1*$^{del\text{-}HDR}$ larvae showed significantly faster response to noxious heat
810 stimulation of 42°C compared to the corresponding control animals of *Canton-S*
811 (average latency of 1.29 ± 0.78 sec in *RluA-1*$^{-/-}$, n=54 vs. 2.22 ± 1.32 sec in *CS*, n=39),
812 *w*^{1118} (2.23 ± 1.57 sec in *RluA-1*$^{-/-}$, n=51 vs. 4.16 ± 2.31 sec in *w*^{1118}, n=36) and iso*w*^{1118}
813 (4.82 ± 2.53 sec in *RluA-1*$^{-/-}$, n=30 vs. 11.99 ± 3.98 sec in iso*w*^{1118}, n=17). Significance of
814 comparisons are marked as **** (p<0.0001). Data were analyzed using Mann-Whitney
815 non-parametric test. **(C).** Transheterozygote *RluA-1*$^{del\text{-}HDR}$/*RluA-1*$^{del\text{-}FRT}$ showed
816 hypersensitive thermal nociception responses compared to the controls (average latency
817 of 3.07 ± 1.72 sec in *RluA-1*$^{del\text{-}HDR}$/*RluA-1*$^{del\text{-}FRT}$, n=195 vs. 6.17 ± 3.95 sec in +/+, n=125).
818 The genetic background is *w*^{1118} for *RluA-1*$^{del\text{-}HDR}$, and iso*w*^{1118} for *RluA-1*$^{del\text{-}FRT}$. For the
819 *RluA-1*$^{del\text{-}HDR}$/*RluA-1*$^{del\text{-}FRT}$ transheterozygotes, data were pooled from the progeny from
820 reciprocal crosses of *RluA-1*$^{del\text{-}HDR}$ to *RluA-1*$^{del\text{-}FRT}$. To generate the control larvae,
821 reciprocal crosses were made between the genetic background of *w*^{1118} and iso*w*^{1118} and

822 the data from the progeny of these crosses were pooled. Significance of the comparison
823 is marked as **** (exact p<0.0001). Data were analyzed using Mann-Whitney U test.
824 **Figure 3**: ***RluA-1* nociception phenotypes with (A) chromosome duplication or (B)**
825 **Class IV-specific expression of *UAS-RluA-1 cDNA*.** (**A**). The hypersensitive nociception
826 phenotype with 42°C thermal stimulus in *RluA-1*$^{del\text{-}HDR}$ null mutant was rescued by
827 introducing a duplication (Dp) on the third chromosome which covers the *RluA-1* gene
828 region (average latency of 8.02 ± 3.61 sec in *RluA-1*$^{-/-}$; Dp/Dp, n=38, which is similar to
829 the iso*w*^{1118} genetic background (+/+, average latency of 10.16±3.87 sec, n=22) , but
830 significantly slower than the latency of 5.31 ± 2.16 sec in *RluA-1*$^{-/-}$, n=34 (p=0.02)). Larvae
831 with one copy of duplication showed slower response (average latency of 6.90 ± 4.81
832 sec in *RluA-1*$^{-/-}$*; Dp/+*, n=45) without statistical significance compared to *RluA-1*$^{del\text{-}HDR}$.
833 Data were analyzed using Kruskal-Wallis test with Dunn's multiple comparison tests. (**B).**
834 The hypersensitive thermal nociception phenotype in *RluA-1*$^{del\text{-}HDR}$ larvae was completely
835 reversed to that of the heterozygous *RluA-1* by Class IV specific expression of full length
836 *RluA-1-cDNA* (*RluA-1*$^{-/-}$*; ppk-Gal4*$^{+/-}$*; UAS-RluA-1*$^{+/-}$, average latency of 12.37 ±6.48 sec,
837 n=30, is similar to *RluA-1*$^{+/-}$*; ppk1.9-Gal4*$^{+/-}$, average latency of 11.04 ± 5.44 sec, n=20
838 but significantly slower than either the driver alone (*RluA-1*$^{-/-}$*; Ppk1.9-Gal4*$^{+/-}$, average
839 latency of 3.78±2.11 sec, n=25 or transgene alone controls (*RluA-1*$^{-/-}$*; UAS-RluA-1*$^{+/-}$,
840 average latency of 2.86 ± 1.39 sec, n=33) at 42°C thermal stimulus. Significance of the
841 comparisons are marked as **** (p<0.0001). Data were analyzed using Kruskal-Wallis test
842 with Dunn's multiple comparison tests.

843 **Figure 4**: ***RluA-1* mechanical nociception and gentle touch responses.** (**A**). In response
844 to the noxious mechanical stimulus of 30mN/720kPa, all (100%) of the *RluA-1*$^{del\text{-}HDR}$ null
845 mutant larvae (*RluA-1*$^{-/-}$, n=28) rolled compared to the 78.57% of control larvae (iso*w*^{1118}
846 n=28) rolling. At the reduced stimulus of 15mN/360kPa, 95.56% of *RluA-1*$^{-/-}$ (n=45) rolled
847 while only 48.53% of control (n=68) rolled. Significance of the comparisons are marked
848 as *($p<0.05$) and **** ($p<0.0001$). Data were analyzed using Fisher's exact test and
849 presented as percentages ± 95% confidence intervals. (**B**). *RluA-1*$^{del\text{-}HDR}$ larvae (*RluA-1*$^{-/-}$)
850 had a gentle touch response score (6.70 ± 2.48, n=36) similar to the control larvae
851 (iso*w*^{1118}, 7.83 ± 2.69, n=30). ns, not significant ($p>0.05$). Data were analyzed with
852 Student's t test.

853 **Figure 5**: **RluA-2 expression in *Drosophila* larvae.** (**A**). In third instar larvae of *RluA-2-*
854 *GFSTF* line, anti-GFP (green) immunoreactive signals are detected in the nuclei of all
855 types of cells (neurons are labelled with anti-HRP (red)). Scale bar = 100μm. **(B).** In the
856 larval abdominal dorsal PNS cluster of *RluA-2-GFSTF* line, GFP signal (green) is also
857 detected in the nuclei of the md neurons, whose membranes are marked with anti-HRP
858 (magenta). Arrow points to Class IV ddaC neuron. Scale bar = 50μm.

859 **Figure 6**. **Thermal nociception responses of *RluA-1* and *RluA-2* single mutant, and**
860 ***RluA-1 RluA-2* double mutant**. Larvae of single mutant *RluA-1*$^{del\text{-}HDR}$ (*RluA-1*$^{-/-}$), *RluA-2*$^{del\text{-}}$
861 ^{HDR} (*RluA-2*$^{-/-}$), double mutant *RluA-1*$^{del\text{-}HDR}$ *RluA-2*$^{del\text{-}HDR}$ (*RluA-1*$^{-/-}$ *RluA-2*$^{-/-}$) and the genetic
862 background iso*w*^{1118} (+/+) were stimulated with noxious heat probe of 42°C. *RluA-1*$^{-/-}$,
863 *RluA-2*$^{-/-}$, and *RluA-1*$^{-/-}$ *RluA-2*$^{-/-}$ all displayed faster responses to the stimulus compared to
864 controls (*RluA-1*$^{-/-}$ average latency of 4.32 ± 2.80 sec, n= 79; *RluA-2*$^{-/-}$, 6.63 ± 3.31 sec,

865 n=68; (*RluA-1*$^{-/-}$*RluA-2*$^{-/-}$), 6.26 ± 3.46 sec, n=57; +/+, 13.72 ± 6.03 sec, n=46). Significance
866 of comparisons are marked as ** (p<0.01), *** (p<0.001) or **** (p<0.0001). Data were
867 analyzed using Kruskal-Wallis test with Dunn's multiple comparison tests.

868 **Figure 7**. ***RluA-1* ddaC neuron dendrite morphology.** (**A-C).** Quantification of the
869 branch number (**A**), average branch length (**B**), and isoneuronal cross-over points (**C**). (**A).**
870 Homozygous *RluA-1*$^{del\text{-}HDR}$ larvae showed a higher normalized branch number (total
871 number of branches / (neuron size x $10^{-4}\mu m^2$), 32.56 ± 7.83 in *RluA-1*$^{-/-}$; *ppk-tdTom*, n=6
872 vs 23.10 ± 4.96 in *ppk-tdTom* control, n=6, p<0.05). (**B).** The mean ddaC dendritic branch
873 length in homozygous *RluA-1*$^{del\text{-}HDR}$ was shorter than that of the control (average branch
874 length is 14.01 ± 1.29 μm in *RluA-1*$^{-/-}$; *ppk-tdTom*, n=6 vs 16.30 ± 1.07 μm in *ppk-tdTom*
875 control, n=6, p<0.01). (**C).** The number of ddaC dendritic isoneuronal crossovers
876 in homozygous *RluA-1*$^{del\text{-}HDR}$ was higher compared to that of the control (normalized
877 crossover points = crossover points / (neuron size x 10^{-7} μm^2), 25.03 ± 8.24 in *RluA-1*$^{-/-}$;
878 *ppk-tdTom*, n=6 vs 13.48 ± 4.08 in *ppk-tdTom* control, n=6, p<0.05). Significant
879 differences are marked as * (p<0.05) and ** (p<0.01). Data were analyzed with Student's
880 t test. (**D).** Representative traced dendritic structure of a class IV ddaC neuron of an L3
881 larva expressing *ppk-GAL4* > *UAS-td-Tom* in homozygous *RluA-1*$^{del\text{-}HDR}$ (*RluA-1*$^{-/-}$, **left**) in
882 comparison with that of the *ppk-tdTom* control (+/+, **right**). The position of the cell body
883 is marked with blue circle and axon with red circles.

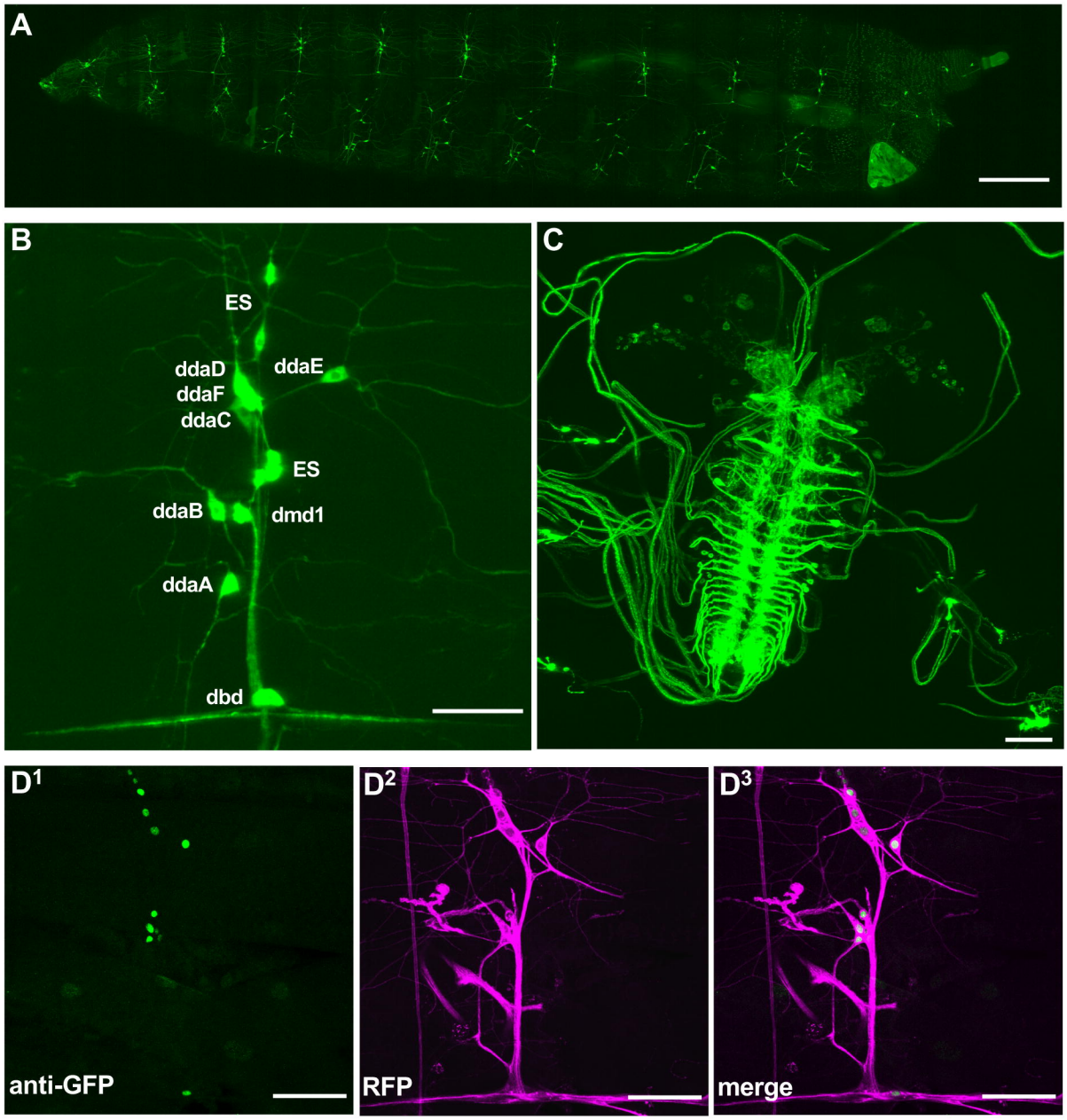
A
B
ES
ddaD
ddaE
ddaF
ddaC
ES
ddaB
dmd1
ddaA
dbd
C
D1
anti-GFP
D2
RFP
D3
merge

Figure 1

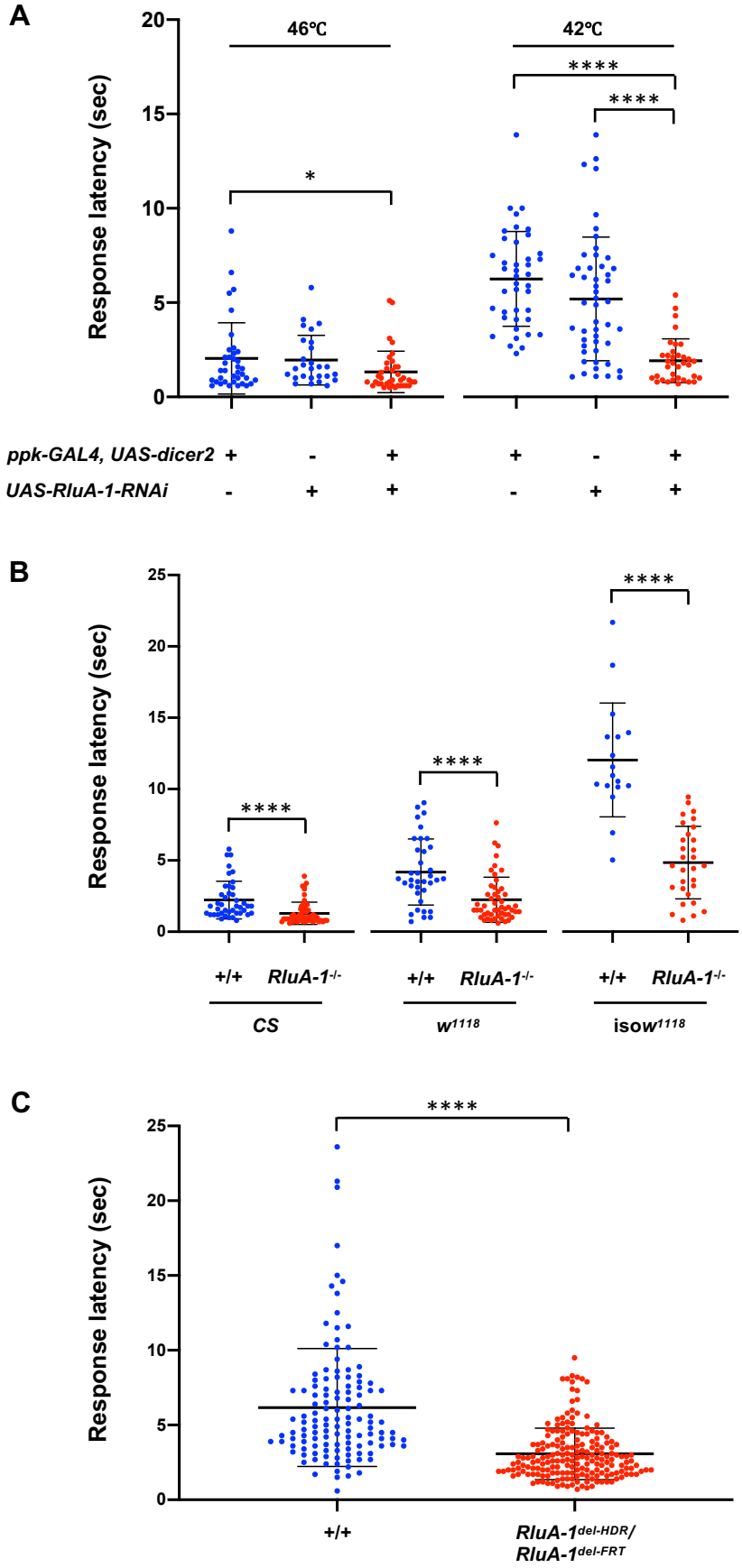
A
46℃
42℃
Response latency (sec)
20
15
10
5
0
*
****
****
ppk-GAL4, UAS-dicer2 + - + + - +
UAS-RluA-1-RNAi - + + - + +
B
Response latency (sec)
25
20
15
10
5
0
****
****
****
+/+ RluA-1-/-
CS
+/+ RluA-1-/-
w1118
+/+ RluA-1-/-
isow1118
C
Response latency (sec)
25
20
15
10
5
0
****
+/+
RluA-1del-HDR/
RluA-1del-FRT

Figure 2

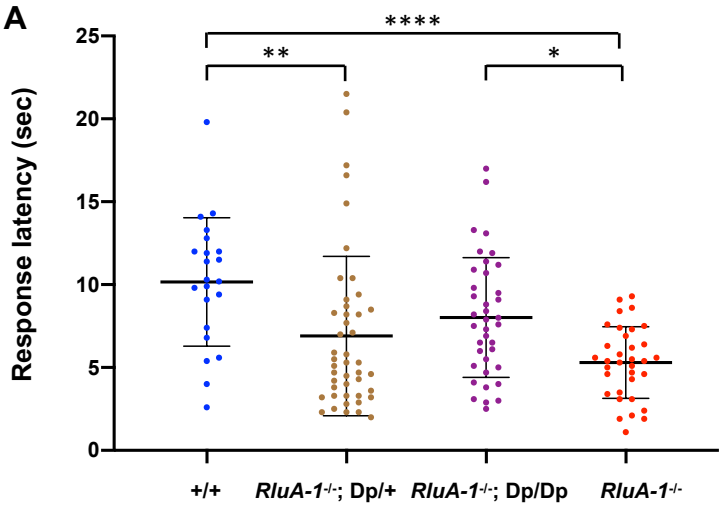
A
Response latency (sec)
25
20
15
10
5
0
****
**
*
+/+
RluA-1-/-; Dp/+
RluA-1-/-; Dp/Dp
RluA-1-/-

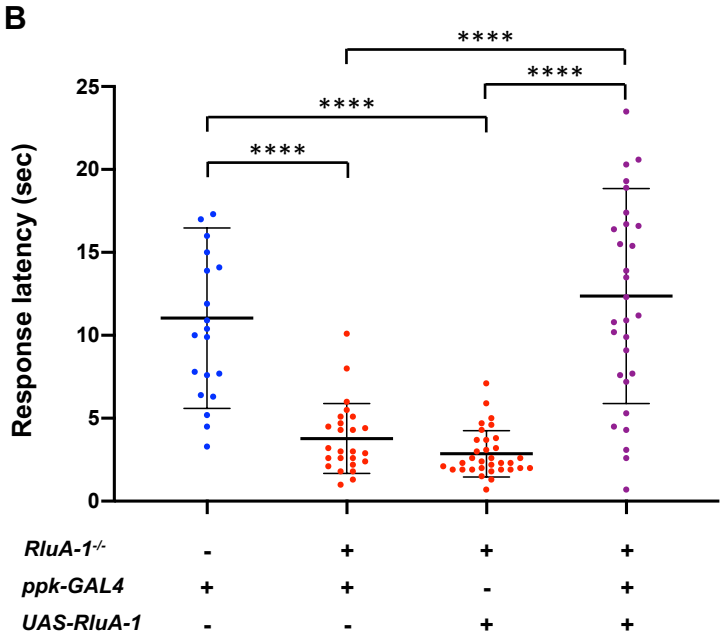
B
Response latency (sec)
25
20
15
10
5
0
****
****
****
****
RluA-1-/- - + + +
ppk-GAL4 + + - +
UAS-RluA-1 - - + +

Figure 3

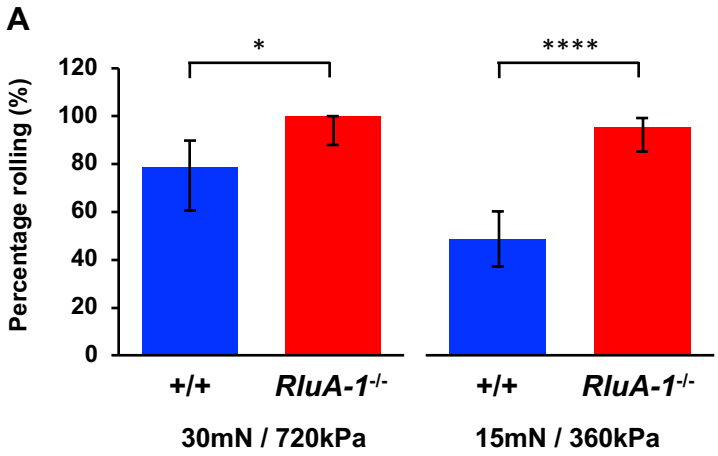
A
*
****
120
100
80
60
40
20
0
Percentage rolling (%)
+/+
RluA-1-/-
+/+
RluA-1-/-
30mN / 720kPa
15mN / 360kPa

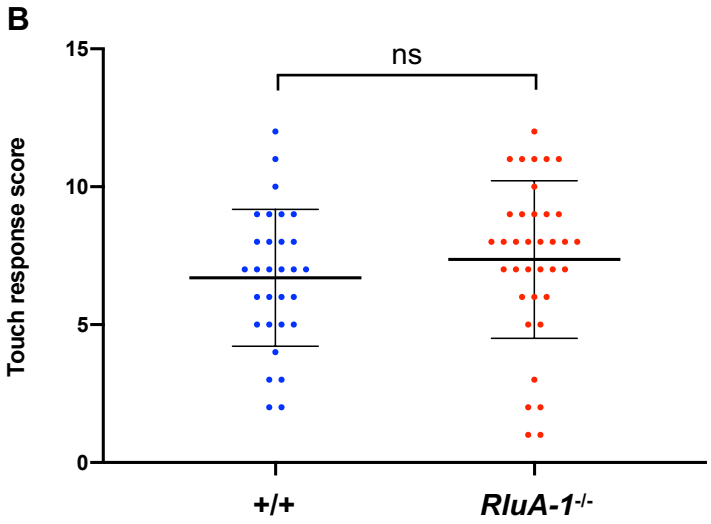
B
ns
15
10
5
0
Touch response score
+/+
RluA-1-/-

Figure 4

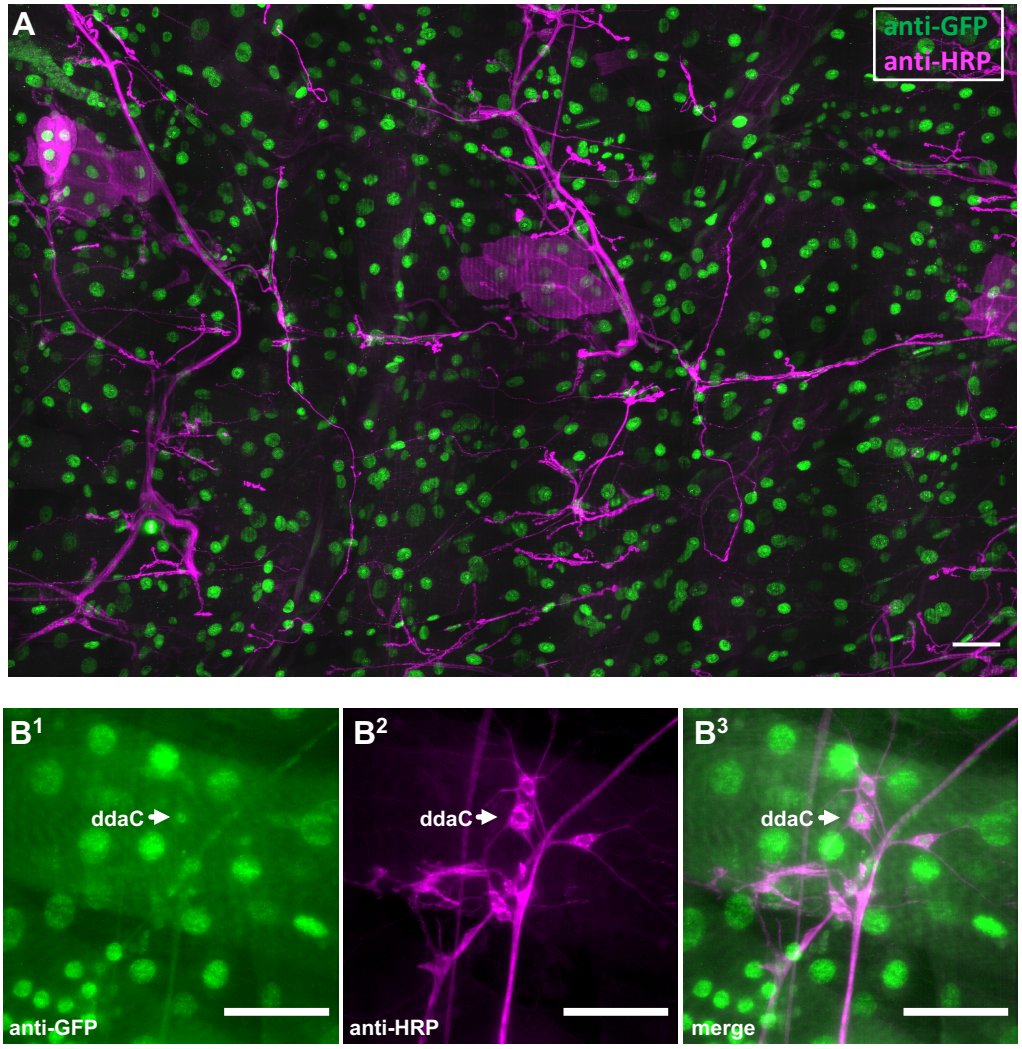
A
anti-GFP
anti-HRP
B1
ddaC
anti-GFP
B2
ddaC
anti-HRP
B3
ddaC
merge

Figure 5

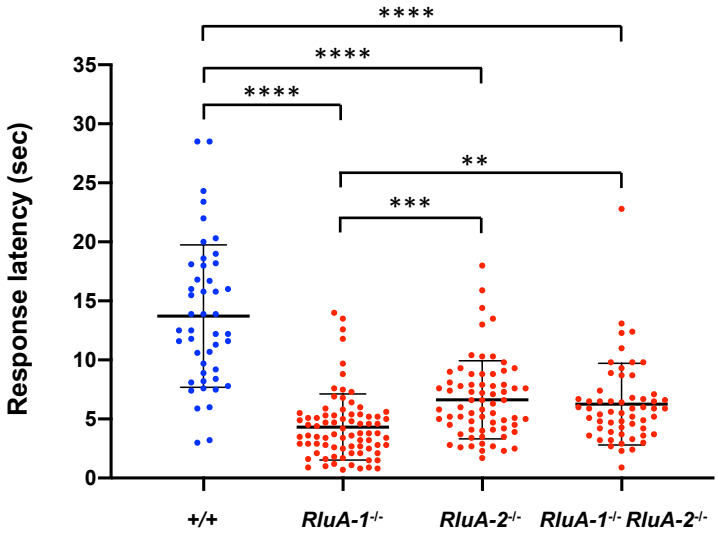
****
****
****
**
***
Response latency (sec)
35
30
25
20
15
10
5
0
+/+
RluA-1-/-
RluA-2-/-
RluA-1-/- RluA-2-/-

Figure 6

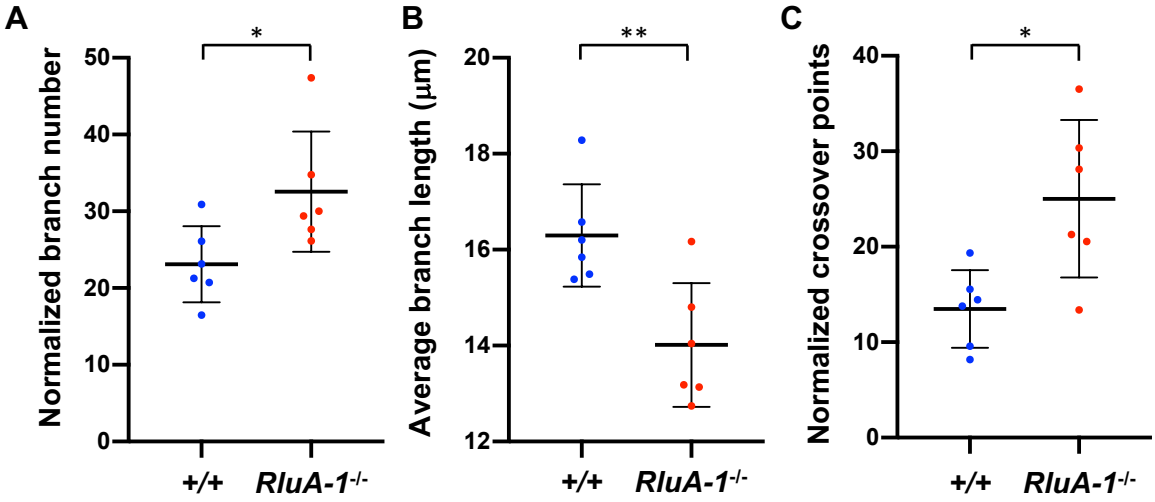
A
Normalized branch number
50
40
30
20
10
0
*
+/+
RluA-1-/-
B
Average branch length (μm)
20
18
16
14
12
**
+/+
RluA-1-/-
C
Normalized crossover points
40
30
20
10
0
*
+/+
RluA-1-/-

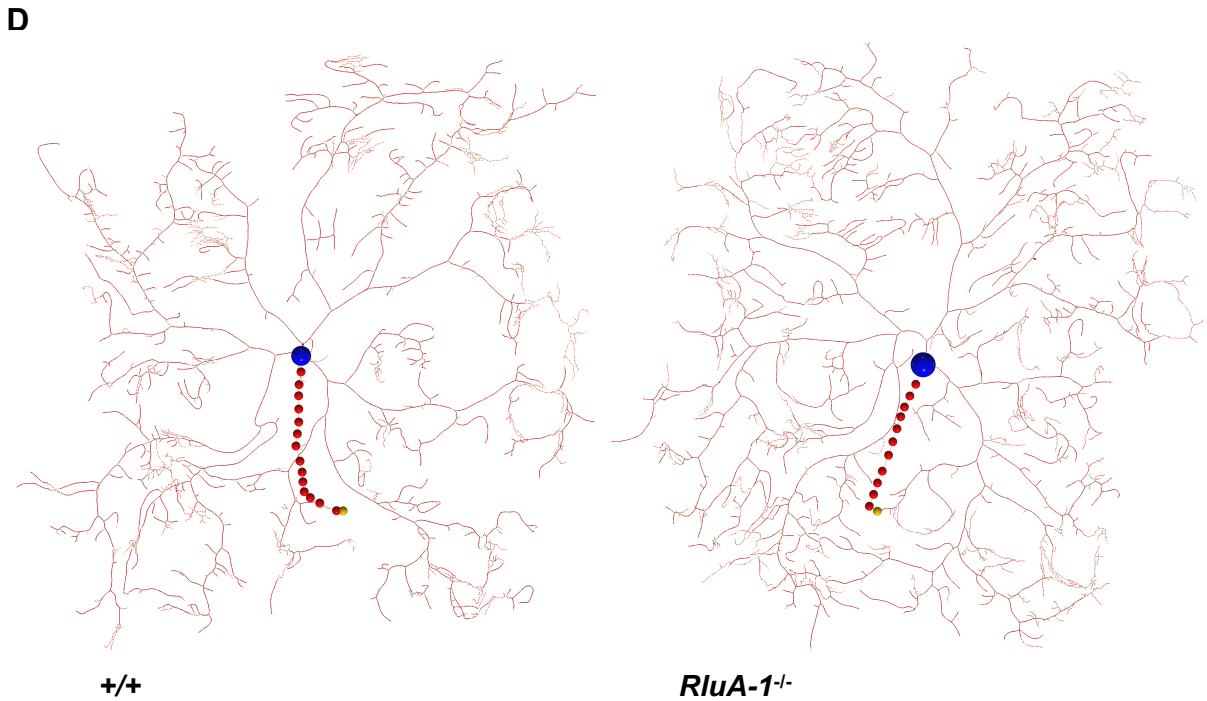
D
+/+
RluA-1-/-

Figure 7